UNIVERSITÀ
DEGLI STUDI
DI PADOVA

University of Padua
Department of Mathematics "Tullio Levi-Civita"
DOCTORAL SCHOOL IN MATHEMATICAL SCIENCES
CURRICULUM MATHEMATICS
CICLE XXXVI

Continuum Modelling and Simulation for Viscoelastic Materials

PhD Candidate: Muhanna Ali H Alrashdi

Supervisor: Prof. Giulio Giuseppe Giusteri

Abstract

A class of continuum mechanical models aimed at describing the behaviour of viscoelastic fluids by incorporating concepts originated in the theory of solid plasticity is introduced. Within this class, even a simple model with constant material parameters is able to qualitatively reproduce a number of experimental observations in both simple shear and extensional flows, including linear viscoelastic properties, the rate-dependence of steady-state material functions, the stress overshoot in incipient shear flows, and the difference in shear and extensional rheological curves. Furthermore, by allowing the relaxation time of the model to depend on the total strain, we can reproduce some experimental observations of the non-attainability of steady flows in uniaxial extension, and link this to a concept of polymeric jamming or effective solidification. Numerical simulations are presented to further illustrate the properties of the proposed model.

Contents

Introduction

Rheology deals with the way materials deform when forces are applied to them. The subject of its studies comprises both fluid-like and solid-like behaviors, that can appear in combination when dealing with complex fluids. At opposite ends of the viscoelastic spectrum we find Newtonian viscous fluids and elastic solids. The former resist shear by dissipating energy and can strain indefinitely under an applied stress, the latter can store energy and balance the applied stress to reach a static configuration, always remembering their original shape. To be able to describe intermediate material responses, we need to address the evolution of the elastically relaxed shape, as well as that of the actual deformation.

Viscoelastic models in continuum mechanics go all the way back to Maxwell and reached a fundamental turning point in their systematic treatment with the work of Oldroyd. In the approach of differential models, the flow equations are typically coupled to an evolution equation for either the elastic stress itself or a conformation tensor. The time-dependence of the elastically relaxed shape is implicit in these relations. Oldroyd's contributions to complex fluid modeling extended beyond his seminal 1950 work [1], notably with a 1958 paper [2] that led to the development of the Oldroyd 8-constant model. This model incorporated parameters allowing for smooth interpolation between the Oldroyd-A and Oldroyd-B models [2]. Johnson and Segalman further exploited this concept in a reduced Oldroyd A/B framework [3]. In 1963, White and Metzner extended the upper-convected Maxwell (UCM) model [4], while Giesekus combined various theories in his 1966 work on modelling elastic effects in liquids [5]. Bird and Carreau transformed the UCM model into an integral one, leading to the Bird–Carreau generalized Newtonian model [6]. Marrucci connected viscoelastic flow to nonequilibrium thermodynamics in 1972 [7], bringing a more microscopic perspective to the subject. Nearly at the same time, Gordon and Showalter developed a 4-parameter model based on microscopic kinetic theory [8]. Acierno *et al.* proposed a model for dense polymer networks, considering several nonlinear effects [9]. Additionally, the Phan-Thien and Tanner model was introduced to describe concentrated polymer solutions and melts [10, 11]. A very informative review of Oldroyd's influence on complex fluids modelling can be found in a recent article by Beris [12] and several textbooks are available on the topic (see, for instance, [13–15]).

In this work, we wish to approach the modelling of viscoelastic materials in a somewhat different way, by combining concepts coming from the theory of solid plasticity with a fluid mechanics framework. Our goal is to capture the behavior of viscoelastic fluids measured

in experiments with constitutive models in which the material parameters have a clear mechanical meaning. Even though we will present a general approach to the modelling of viscoelastic materials, our main objective is to capture properties of polymeric solutions and we will address typical effects such as the stress overshoot in start-up flows, shear thinning, stress relaxation, and the difference between shear and extensional rheology.

We will present a framework in which viscoelastic fluids emerge as an interpolation between purely viscous fluids and solids, controlled by a relaxation time parameter ranging from zero (viscous fluid) to infinity (viscoelastic solid). We will shown that a simple model with constant material parameters performs very well in reproducing the behavior of polymer solutions observed in rheometric experiments. Moreover, our approach helps understanding the origin of the difference in extensional and shear rheology and the relative importance of viscous, elastic, and plastic effects.

We will also exemplify the use of our framework to fit rheological data about wormlike micellar solutions (WLMs). Wormlike micelles are long, semi-flexible cylindrical aggregates with viscoelastic properties similar to polymer molecules [16–18]. WLMs are a system that lives in a dynamic equilibrium since the long aggregates undergo scission and recombination processes that contribute to stress relaxation mechanisms and flow-induced morphological changes [19, 20]. They are extensively used in industry, thanks to their tunable properties, in the context of drag reduction, oil recovery, cosmetics, personal care, and food products [21–24]. Rheological studies show that WLMs exhibit linear viscoelastic behavior describable by a single-mode Maxwellian relaxation spectrum, with more complex behavior under large deformations [21, 25, 26]. Under certain conditions, WLM solutions display a stress plateau in the flow curve, indicative of shear banding phenomena where broken, short, and aligned micelles form a high-shear-rate band near the moving wall, while unbroken entangled micelles form a low shear rate band near the fixed wall. At very high shear rates, all micelles break, and the solution behaves like a Newtonian fluid, resulting in a non-monotonic flow curve and hysteresis [27]. Additionally, experiments suggest extension hardening followed by extension thinning in WLMs under uniaxial and planar extension [28–30].

In Chapter 1, we recall some general concepts regarding the rheological characterization of non-Newtonian fluids and the classical framework of continuum tensorial models for their behaviour. The second chapter contains the description of our proposal and evidence of its effectiveness in capturing some fundamental features of the rheology of viscoelastic fluids. In Chapter 3, we present numerical simulations of flows in two-dimensional domains to further illustrate the properties of our model.

Chapter 1

Rheological characterization of viscoelastic fluids

In this chapter we recall some well-known facts and concepts regarding the rheological study of viscoelastic fluids. More detailed presentations and discussions of experimental techniques can be found in several textbooks and review papers (see for instance [12–15, 31] and the references therein).

The basic balance equations of continuum mechanics are the continuity equation

$$\mathcal{D}_{\boldsymbol{u}}\rho + \rho \operatorname{div} \boldsymbol{u} = 0, \tag{1.1}$$

and the balance of linear momentum:

$$\rho \mathcal{D}_{\boldsymbol{u}} \boldsymbol{u} = \operatorname{div} \boldsymbol{\sigma} + \rho \boldsymbol{b}, \tag{1.2}$$

where ρ is the mass density, $\boldsymbol{u}$ is the velocity field, $\boldsymbol{b}$ is the density of external forces per unit mass, and $\boldsymbol{\sigma}$ is the Cauchy stress tensor. For the sake of clarity, we use

$$\mathcal{D}_{\boldsymbol{u}} := \frac{\partial}{\partial t} + \boldsymbol{u} \cdot \nabla$$

to denote the material time derivative.

For incompressible materials $\operatorname{div} \boldsymbol{u} = 0$, ρ is constant, and we write $\boldsymbol{\sigma} = -p\mathsf{I} + \mathsf{T}$ where the pressure p multiplies the identity matrix I and T is the extra stress. Developing a material model consists in finding a suitable relation between $\boldsymbol{\sigma}$ and the other fields that describe the system. Finding suitable constitutive equations for non-Newtonian fluids is a significant difficulty in the science of rheology, as T for polymers and other non-Newtonian fluids is a far more complex function of material parameters than for Newtonian fluids.

Standard flows are used in materials investigations to find constitutive equations. In what follows, we present basic shear flows and extensional flows and the material functions that can be measured from them. The material under study and the kind of flow applied to it determine the stress responses that are seen. Generally speaking, the responses will rely on the chemical makeup of the material and will be factors of time, strain, strain rate, or other kinematic characteristics associated with the flow.

1.1 Simple shear flows

The following is the definition of the velocity profile for simple shear flow in Cartesian coordinates:

$$\boldsymbol{u} = \begin{pmatrix} u_1 \\ u_2 \\ u_3 \end{pmatrix} = \begin{pmatrix} \dot{\gamma}(t)x_2 \\ 0 \\ 0 \end{pmatrix} \tag{1.3}$$

The flow direction of shear flow in Cartesian coordinates is commonly chosen as the 1-direction, with the gradient direction, the 2-direction, designating the direction in which the velocity changes and the 3-direction being the vorticity direction.

The shear-rate tensor $\mathsf{D} = \frac{1}{2}(\nabla \boldsymbol{u} + (\nabla \boldsymbol{u})^{\mathsf{T}})$ for this class of flows reads

$$\mathsf{D} = \frac{\dot{\gamma}(t)}{2} \begin{pmatrix} 0 & 1 & 0 \\ 1 & 0 & 0 \\ 0 & 0 & 0 \end{pmatrix}. \tag{1.4}$$

The shear rate, also known as the rate of strain, is the magnitude of $\dot{\gamma}$ for shear flows, while the sign of $\dot{\gamma}$ affects the direction of the flow. Simple shear flows are homogeneous because the velocity gradient is independent of the position.

If we now consider the simple Newtonian constitutive equation, we have

$$\mathsf{T} = 2\eta\mathsf{D}. \tag{1.5}$$

Of the nine Cartesian components of the stress tensor, for a Newtonian incompressible fluid in shear flow only two are nonzero and these two components are equal, leading to the relation

$$\mathsf{T}_{12} = \mathsf{T}_{21} = 2\eta\mathsf{D}_{12} = \eta\dot{\gamma}(t) = \eta\frac{\partial u_1}{\partial x_2} \tag{1.6}$$

This formula represents the well-known Newton's law of viscosity [32]. The viscosity $\eta = \mathsf{T}_{12}/\dot{\gamma}$ can be computed using the shear stress T_{12} and the imposed deformation rate $\dot{\gamma} = \partial u_1/\partial x_2$. This is all the material information required to specify the constitutive equation and, thus, the only quantity one needs to measure in experiments to characterise a Newtonian fluid.

The situation for non-Newtonian fluids is more complicated. Typically, the stress tensor is determined by more than one component and those components are functions of kinematic factors such as $\dot{\gamma}$ rather than being constant. Here below we recall standard material functions and experiments [33] used for the rheological characterization of non-Newtonian fluids.

1.1.1 Small-amplitude oscillatory flows

Small-amplitude oscillatory shear (SAOS) is used to characterize the linear viscoelastic properties of complex materials. This is an unsteady shear flow with periodic shear-rate

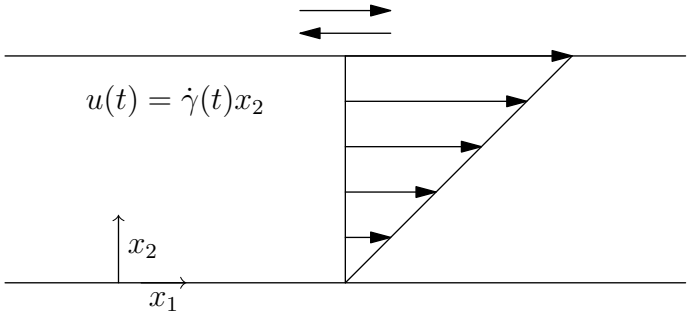

Figure 1.1: Schematics of SAOS with amplitude γ_0 and frequency ω.

function $\dot{\gamma}(t)$ (see Figure 1.1), with

$$\boldsymbol{u} = \begin{pmatrix} \dot{\gamma}(t)x_2 \\ 0 \\ 0 \end{pmatrix} \qquad \text{and} \qquad \dot{\gamma}(t) = \gamma_0\omega\cos\omega t, \tag{1.7}$$

where ω (rad/s) is the angular frequency of the oscillation, and γ_0 is the strain amplitude. Usually, a parallel plate or cone-and-plate torsional rheometer is used to measure this flow, but measurements can be performed with the rotary Couette rheometer as well.

The shear strain corresponding to this flow is indeed given by $\gamma(t) = \gamma_0 \sin\omega t$. This kind of straining a sample at low strain amplitudes will result in a shear stress that is a sine wave with the same frequency as the input strain wave. However, the shear stress and the input strain are typically out of phase. This leads to the expression

$$\mathsf{T}_{12}(t) = \mathsf{T}_0 \sin(\omega t + \delta) \tag{1.8}$$

where the phase difference between the strain wave and the stress response is given by the quantity δ. Such a sinusoidal shear stress output serves as the basis for defining the material functions for SAOS. Trigonometric identities allow us to write

$$\mathsf{T}_{12}(t) = (\mathsf{T}_0\cos\delta)\sin\omega t + (\mathsf{T}_0\sin\delta)\cos\omega t. \tag{1.9}$$

We observe that one part of the shear stress oscillates in phase with the applied strain, proportional to $\sin\omega t$, and a second part in phase with the shear rate, proportional to $\cos\omega t$. The first term resembles the response of a purely elastic solid, while the second term would be the response of a purely viscous fluid. Equation 1.9 describes the stress response in SAOS as having two parts: an elastic part (proportional to γ_{21}) and a Newtonian-like part (proportional to $\dot{\gamma}_{21}$). As a result, the SAOS experiment is perfect for examining materials that exhibit both elastic and viscous characteristics, or viscoelastic materials.

The storage modulus $G^{'}(\omega)$ and the loss modulus $G^{''}(\omega)$ are the material functions for SAOS, and they are defined by

$$\frac{\mathsf{T}_{12}}{\gamma_0} = G^{'}(\omega)\sin\omega t + G^{''}(\omega)\cos\omega t, \tag{1.10}$$

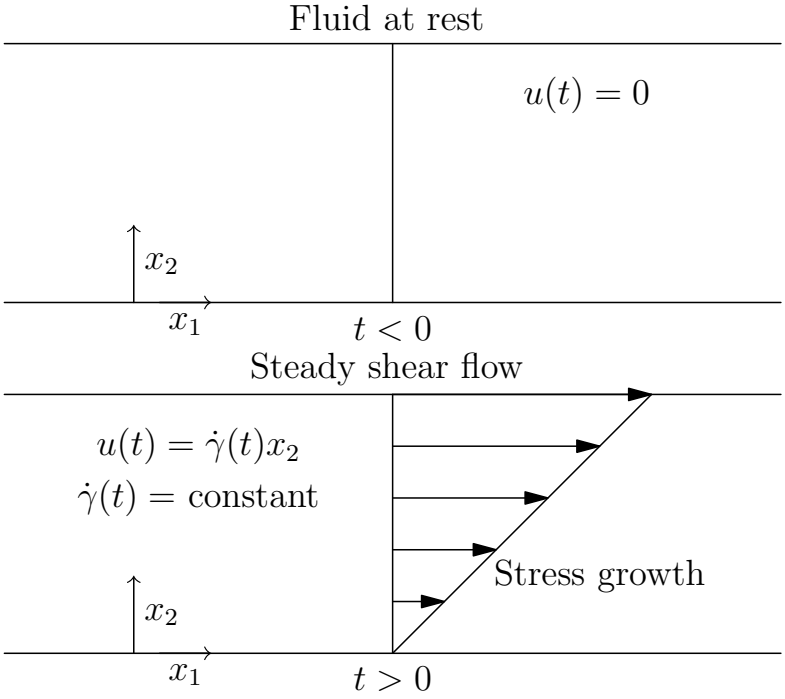

Figure 1.2: Schematics of start-up flows: when $u(t) = 0$ the fluid is rest and when the top plate starts moving the stress grows.

that gives

$$G^{'}(\omega) = \frac{\mathsf{T}_0}{\gamma_0} \cos\delta, \tag{1.11}$$

$$G^{''}(\omega) = \frac{\mathsf{T}_0}{\gamma_0} \sin\delta. \tag{1.12}$$

1.1.2 Stress growth in simple shear

The most popular rheological measurements are viscosity measurements, which are done in steady-state flow. However, there is a start-up phase to the experiment where the stress increases from zero to the steady-state value. In this flow, $\dot{\gamma}(t)$ is zero for negative times and equals a constant $\dot{\gamma}$ for positive times (see Figure 1.2). In reality, at the very beginning of the motion there is a transient regime in which the flow is not homogeneous. The imposed shear stress propagates from the upper boundary and it is only when the velocity profile becomes linear that we achieve a simple shear flow with the given rate.

Three time-dependent stress values, the shear stress $\mathsf{T}_{12}(t, \dot{\gamma})$ and the first and second normal stress differences $\mathsf{N}_1(t, \dot{\gamma}) = \mathsf{T}_{11} - \mathsf{T}_{22}$, and $\mathsf{N}_2(t, \dot{\gamma}) = \mathsf{T}_{22} - \mathsf{T}_{33}$, will be used to

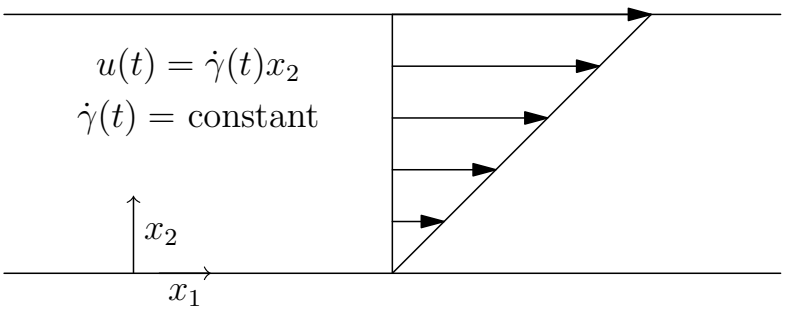

Figure 1.3: When we shear for long time we reach a steady-state with constant shear stress.

quantify how a general fluid responds to this flow. The relevant material functions are:

$$\text{Shear viscosity:} \qquad \eta^+(t,\dot{\gamma}) = \frac{\mathsf{T}_{12}(t,\dot{\gamma})}{\dot{\gamma}}; \tag{1.13}$$

$$\text{First normal stress coefficient:} \qquad \Psi_1^+(t,\dot{\gamma}) = \frac{\mathsf{N}_1(t,\dot{\gamma})}{\dot{\gamma}^2}; \tag{1.14}$$

$$\text{Second normal stress coefficient:} \qquad \Psi_2^+(t,\dot{\gamma}) = \frac{\mathsf{N}_2(t,\dot{\gamma})}{\dot{\gamma}^2}. \tag{1.15}$$

As indicated above, all of these material functions are generally dependent on both time and the applied shear rate $\dot{\gamma}$.

1.1.3 Steady Shear flow

A steady shear flow is reached under a constant $\dot{\gamma}$ when also the stress becomes time-independent. Usually, this flow is monitored by measuring the torque produced by the fluid being tested by rotating a cone or plate at a constant angular velocity using a cone-and-plate or parallel plate geometry. The material functions for steady shear can be defined from the startup flow material functions as

$$\eta(\dot{\gamma}) = \lim_{t\to\infty} \eta^+(t,\dot{\gamma}), \tag{1.16}$$

$$\Psi_1(\dot{\gamma}) = \lim_{t\to\infty} \Psi_1^+(t,\dot{\gamma}), \tag{1.17}$$

$$\Psi_2(\dot{\gamma}) = \lim_{t\to\infty} \Psi_2^+(t,\dot{\gamma}). \tag{1.18}$$

1.1.4 Stress relaxation

The fact that polymers and other viscoelastic materials have partial memory that is, the stresses they cause do not relax right away but instead gradually decay is one of their main characteristics. The stress relaxation experiment in shear flow is used to look at relaxation times. In this experiment, a sample resting between parallel plates is abruptly disturbed, for a brief period of time Δ, by the application of a constant and large shear rate (see Figure 1.4).

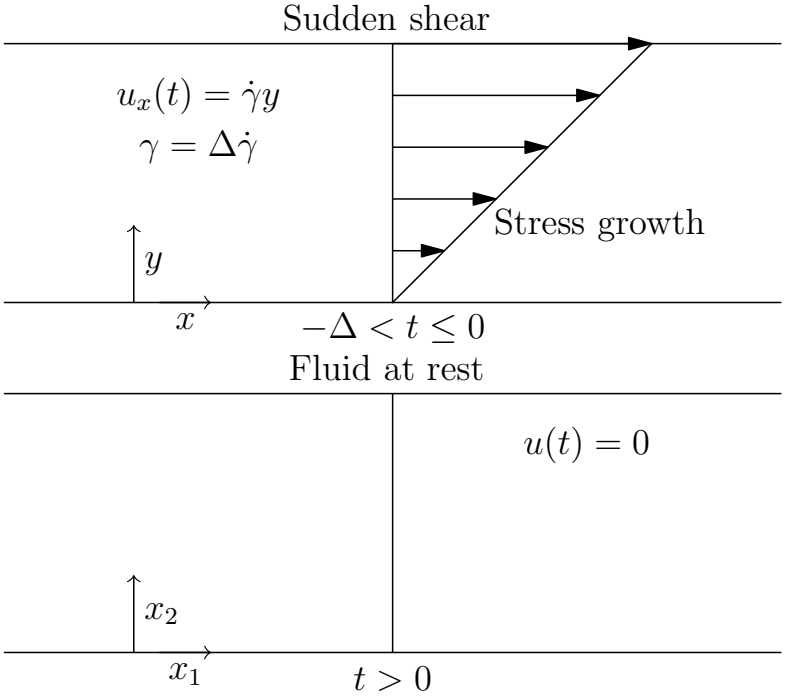

Figure 1.4: In relaxation experiments the fluid is at rest after a sudden shear.

A non-Newtonian fluid experiences a sharp rise in shear stress and possibly in normal stress differences. The material functions for the step-strain experiment are based on the concept of modulus, which is the ratio of stress to strain. Generally speaking, depending on the coordinate system selected, the strain γ could be positive or negative. The coordinate system that we use will ensure that γ is positive.

The material functions for stress relaxation are:

$$\text{Relaxation modulus :} \qquad G(t,\gamma) = \frac{\mathsf{T}_{12}(t,\gamma)}{\gamma}; \tag{1.19}$$

$$\text{First normal stress relaxation modulus :} \qquad G_{\Psi_1}(t,\gamma) = \frac{\mathsf{N}_1(t,\gamma)}{\gamma^2}; \tag{1.20}$$

$$\text{Second normal stress relaxation modulus :} \qquad G_{\Psi_2}(t,\gamma) = \frac{\mathsf{N}_2(t,\gamma)}{\gamma^2}. \tag{1.21}$$

It is important to note that the material functions for the step-strain experiment are functions of both the strain amplitude γ and time. It is observed that $G(t,\gamma)$ and $G_{\Psi_1}(t,\gamma)$ are independent of strain for small strains; this limit is referred to as the linear viscoelastic regime. In the linear viscoelastic domain, $G(t,\gamma)$ is expressed as $G(t)$.

1.2 Extensional flows

Extensional flows are characterized by a velocity gradient that is symmetric, with zero vorticity. One formula for the velocity profile can be used to represent extensional flows in a parametric way [13]:

$$\boldsymbol{u} = \begin{pmatrix} u_1 \\ u_2 \\ u_3 \end{pmatrix} = \begin{pmatrix} -\frac{1}{2}\dot{\epsilon}(t)(1+b)x_1 \\ -\frac{1}{2}\dot{\epsilon}(t)(1-b)x_2 \\ \dot{\epsilon}(t)x_3 \end{pmatrix}. \tag{1.22}$$

In particular, uniaxial extension is obtained with $b = 0$ and $\dot{\epsilon} > 0$, while planar extension is given by $b = 1$ and $\dot{\epsilon} > 0$. We will restrict our attention to the case in which the deformation rate $\dot{\epsilon}$ is constant. Similar to the case of simple shear, we can define time-dependent material functions and their steady-state limit by suitable combinations of stress components and deformation rate. By symmetry considerations it can be shown that only one scalar function characterizes the response in uniaxial extensional flows. It is the uniaxial extensional viscosity given by

$$\eta_{\mathrm{u}}^{+}(t,\dot{\epsilon}) = \frac{\mathsf{T}_{33}(t,\dot{\epsilon}) - \mathsf{T}_{11}(t,\dot{\epsilon})}{\dot{\epsilon}}, \quad \text{with} \quad \eta_{\mathrm{u}}(\dot{\epsilon}) = \lim_{t\to\infty} \eta_{\mathrm{u}}^{+}(t,\dot{\epsilon}). \tag{1.23}$$

In the case of planar extensional flows, two material functions are needed and are the first extensional viscosity

$$\eta_{\mathrm{e}}^{+}(t,\dot{\epsilon}) = \frac{\mathsf{T}_{33}(t,\dot{\epsilon}) - \mathsf{T}_{11}(t,\dot{\epsilon})}{\dot{\epsilon}}, \quad \text{with} \quad \eta_{\mathrm{e}}(\dot{\epsilon}) = \lim_{t\to\infty} \eta_{\mathrm{e}}^{+}(t,\dot{\epsilon}), \tag{1.24}$$

and the second viscosity

$$\eta_{\mathrm{se}}^{+}(t,\dot{\epsilon}) = \frac{\mathsf{T}_{11}(t,\dot{\epsilon}) - \mathsf{T}_{22}(t,\dot{\epsilon})}{\dot{\epsilon}}, \quad \text{with} \quad \eta_{\mathrm{se}}(\dot{\epsilon}) = \lim_{t\to\infty} \eta_{\mathrm{se}}^{+}(t,\dot{\epsilon}). \tag{1.25}$$

We note that for our analysis we will make use of material functions for extensional flows that are equivalent to these but more consistent with the ones defined for simple shear.

1.3 Classical constitutive models

We now recall the basic evolution equations for a general continuum in the Eulerian setting. We assume that the density ρ is constant and uniform. To be able to follow the material deformation, we introduce the placement $\boldsymbol{\varphi}(\boldsymbol{X},t)$ that gives the position at time t of a material point labelled with $\boldsymbol{X}$ and solves the nonlinear equation $\partial_t\boldsymbol{\varphi}(\boldsymbol{X},t) = \boldsymbol{u}(\boldsymbol{\varphi}(\boldsymbol{X},t),t)$, which involves the velocity field $\boldsymbol{u}$. We employ the symbol $\boldsymbol{X}$ for the labels of material points, while $\boldsymbol{x}$ indicates a geometric point in space. We define the Eulerian deformation gradient $\mathsf{F}(\boldsymbol{x},t) := \nabla_{\boldsymbol{X}}\boldsymbol{\varphi}|_{\boldsymbol{X}=\hat{\boldsymbol{\varphi}}(\boldsymbol{x},t)}$ with $\hat{\boldsymbol{\varphi}}$ the spatial inverse of $\boldsymbol{\varphi}$, such that $\boldsymbol{\varphi}(\hat{\boldsymbol{\varphi}}(\boldsymbol{x},t),t) = \boldsymbol{x}$.

The balance of linear momentum gives rise to the evolution equation

$$\rho\mathcal{D}_{\boldsymbol{u}}\boldsymbol{u} = \operatorname{div}\boldsymbol{\sigma} \tag{1.26}$$

for the velocity field, driven by the Cauchy stress tensor $\boldsymbol{\sigma}$. We neglect external forces and recall that incompressibility is expressed by the constraint $\operatorname{div} \boldsymbol{u} = 0$.

Regarding the evolution equation for the deformation gradient F in Eulerian coordinates, it reads

$$\mathcal{D}_{\boldsymbol{u}}\mathsf{F} = (\nabla \boldsymbol{u})\mathsf{F}, \tag{1.27}$$

where we use the matrix multiplication $[(\nabla \boldsymbol{u})\mathsf{F}]_{ij} = \sum_k (\nabla \boldsymbol{u})_{ik}\mathsf{F}_{kj}$. Equation (1.27) is an exact kinematic relation between the velocity and the displacement of fluid elements and does not contain any constitutive assumption. We note that for incompressible deformations $\det \mathsf{F} = 1$. This property is preserved by equation (1.27) thanks to the fact that $\operatorname{tr}(\nabla \boldsymbol{u}) = \operatorname{div} \boldsymbol{u} = 0$.

A continuum model is specified by prescribing constitutive relations between the Cauchy stress $\boldsymbol{\sigma}$ and the kinematic fields that identify the state of the material, such as $\nabla \boldsymbol{u}$ and F. Since we consider incompressible materials, we introduce the pressure field p and take $\boldsymbol{\sigma} = -p\mathsf{I} + \mathsf{T}$, with a pressure term proportional to the identity matrix I and a traceless extra stress T. The latter can be further decomposed as the sum of a viscous contribution T_{vi} plus an elastic one T_{el}, so that $\boldsymbol{\sigma} = -p\mathsf{I} + \mathsf{T}_{\mathrm{vi}} + \mathsf{T}_{\mathrm{el}}$.

1.3.1 Oldroyd-B model

The systematic modelling of viscoelastic fluids proposed by Oldroyd [34] is based on the notion of material frame indifference, for which we refer the reader to classical textbooks, that should be respected by constitutive laws. The practical consequence of this assumption is that we cannot use the material time derivative "as is" in constitutive models, but we need to employ the so-called objective rates.

Oldroyd provides two examples of such rates with the lower-convected derivative

$$\overset{\vartriangle}{\mathsf{T}} = \frac{\partial \mathsf{T}}{\partial t} + (\boldsymbol{u} \cdot \nabla)\mathsf{T} + (\nabla \boldsymbol{u})\mathsf{T} + \mathsf{T}(\nabla \boldsymbol{u})^{\mathsf{T}} \tag{1.28}$$

and the upper-convected derivative

$$\overset{\triangledown}{\mathsf{T}} = \frac{\partial \mathsf{T}}{\partial t} + (\boldsymbol{u} \cdot \nabla)\mathsf{T} - \mathsf{T}(\nabla \boldsymbol{u})^{\mathsf{T}} - (\nabla \boldsymbol{u})\mathsf{T}. \tag{1.29}$$

With these, we can construct two models as follows:

- Oldroyd-A model:
$$\mathsf{T} + \tau_{\mathrm{r}} \overset{\vartriangle}{\mathsf{T}} = 2\eta(\mathsf{D} + \tau \overset{\vartriangle}{\mathsf{D}}). \tag{1.30}$$
- Oldroyd-B model:
$$\mathsf{T} + \tau_{\mathrm{r}} \overset{\triangledown}{\mathsf{T}} = 2\eta(\mathsf{D} + \tau \overset{\triangledown}{\mathsf{D}}). \tag{1.31}$$

The Oldroyd-B model has proven to be more appropriate for polymeric fluids. It can be heuristically derived from two quite different "molecular" hypotheses. The network theory of rubber elasticity, which sees rubber as a network of interwoven elastic strands,

is one of these. Green and Tobolsky [35] developed a theory that can lead to the upper-convected Maxwell model, which corresponds to the Oldroyd-B with $\tau = 0$. But it can be also associated with the theory by Kuhn [36], where a polymer molecule is thought of as a linear elastic spring that is susceptible to both Brownian motion and drag from the surrounding fluid, which is treated as Newtonian.

The Oldroyd-B model might be considered as too basic for the following reasons:

1. A single relaxation time is a quite restrictive assumption. In most polymeric fluids there is a spectrum of relaxation phenomena, as is known from experiments and theoretical arguments [37].

2. Molecules are treated as linearly elastic by both the dumbbell and rubberlike theories. This is not suitable for significant deformations.

3. The interactions between various polymer molecules are not sufficiently taken into account by the model. Entanglements between molecules are present in the majority of polymeric fluids.

1.3.2 Other models

Here we recall other important models that are constructed using objective rates (see also [31] for more information). In all these models it is customary to split the extra stress T into two contributions: the solvent contribution T_s and the polymer contribution T_p.

- Johnson–Segalman model [3]:

$$\mathsf{T}_s = 2\eta\mathsf{D},$$
$$\mathsf{T}_p + \tau_{\mathrm{r}}\left(1 - \frac{\xi}{2}\right)\overset{\nabla}{\mathsf{T}}_p + \tau_{\mathrm{r}}\frac{\xi}{2}\overset{\Delta}{\mathsf{T}}_p = 2\eta_p\mathsf{D}.$$

  According to Gordon and Schowalter [38], the physical interpretation of ξ, a dimensionless material parameter with a range of 0 to 2, is that the corresponding derivatives of stress and deformation relate to a non-affine motion, which in fact describes the end-to-end vector motion of a polymer strand with respect to the continuum's macroscopic motion; in such a case, the strand can slip by transmitting only a portion of its stress to the continuum. As a result, ξ can be thought of as a measurement of the shear tensor's non-affine motion component. When ξ=2, a version of the Oldroyd–A model is recovered and the motion is entirely non-affine. For $\xi = 0$ and $\eta = 0$, we have the upper-convected Maxwell model.

- The Giesekus model [39] adds a quadratic nonlinearity:

$$\mathsf{T}_s = \eta\mathsf{D},$$
$$\mathsf{T}_p + \tau_{\mathrm{r}}\overset{\nabla}{\mathsf{T}}_p + \frac{\alpha\tau_{\mathrm{r}}}{\eta_p}\mathsf{T}_p^2 = 2\eta_p\mathsf{D}.$$

  The zero-shear viscosity η_p, the relaxation time τ_{r}, and the anisotropy of the drag experienced by flowing polymer segments α are the three parameters of this model.

- The Phan-Thien–Tanner model [10] (for a single relaxation mode) introduces a different nonlinear term:

$$\mathsf{T}_s = 2\eta \mathsf{D},$$
$$\mathsf{T}_p + \tau_{\mathrm{r}} \overset{\nabla}{\mathsf{T}}_p + \left(\frac{\tau_{\mathrm{r}}}{\eta_p} \operatorname{tr} \mathsf{T}_p \right) \mathsf{T}_p = 2\eta_p \mathsf{D}.$$

  The presence of multiple relaxation times is then modelled by assuming a sum of polymeric stresses all following similar evolution equations.

Finally, we observe that, due to the form of nonlinear term in the cited models, the extra stress can evolve in a form that is not always traceless. In those cases, we can always subtract the spherical part of the extra stress and reabsorb it in the pressure term. In the modelling framework that we will introduce the extra stress will always be traceless by construction.

Chapter 2

A new class of models

In this chapter, we introduce a tensorial modelling framework for viscoelastic materials. It will lead to a model that features the same number of parameters as the upper-convected Maxwell model, but displays improved linear viscoelastic properties akin to those of the Giesekus model and, most importantly, is able to capture rate-dependent effects in transient shear flows as well as flow-type dependence of the rheological curves. We stress that these desirable features emerge as a consequence of the mechanical framework we employ and are not added to our model by design. This marks a definite conceptual advantage in comparison to more complex multi-parameter models.

The main point of our approach is that we obtain the evolution of the elastic stress as a result of the evolution of the current deformation gradient and of a tensorial description of the local relaxed state. The evolution of the former quantity is fully determined by the continuum kinematics, while the structure of the equation for the relaxed state is similar to the flow rules that are postulated in plasticity theory. Within our framework, viscoelastic fluids emerge as an interpolation between purely viscous fluids and solids, controlled precisely by the characteristic time of the plastic evolution. This is a feature not always present in viscoelastic models, as pointed out by Snoeijer *et al.* [40] in a recent review. To achieve our goals, we use well-established concepts from solid plasticity to address the modelling of viscoelastic fluids and show that one can create a fruitful synergy between the fluid and solid perspectives when modelling complex materials. We offer an alternative to Oldroyd's approach by taking more explicitly into account plastic effects. A second important aspect is the use of logarithmic relations between the elastic stress and the strain measure, akin to the Hencky strain approach. Importance and advantages of logarithmic strains have been discussed in the literature by several authors [41–44], but our motivation for this choice comes from a very specific and fundamental aspect. Stresses represent forces that drive the material deformation and, as such, they naturally belong to a linear space in which it is meaningful to take the sum of different contributions to form the total stress. On the other hand, deformation gradients belong to the multiplicative group of linear transformations and the basic measures of strain—the Cauchy–Green tensors—are Riemannian metric tensors. For all these objects, the algebraic operation of sum does not represent any physically relevant operation and we wish to avoid it in

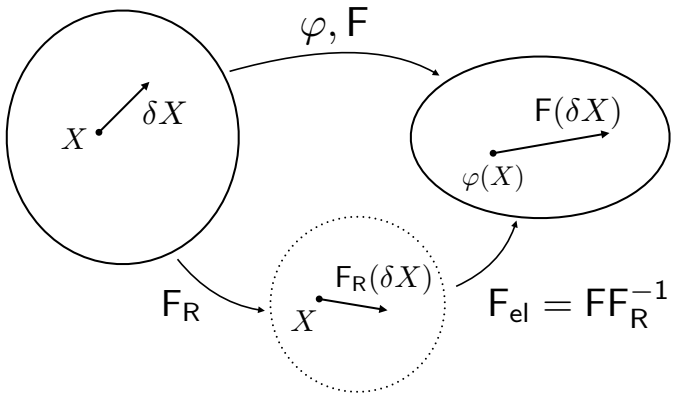

Figure 2.1: Material points $\boldsymbol{X}$ are mapped by the placement $\boldsymbol{\varphi}$ into their position in space, while the deformation gradient F maps tangent vectors $\delta\boldsymbol{X}$ in the material manifold onto spatial vectors. The elastically relaxed state of the material is locally described by F_R, which need not correspond to any global deformation of the material and, in this sense, it maps material vectors onto material vectors. The elastic stresses will then depend upon the mapping $\mathsf{F}_\mathrm{el} = \mathsf{F}\mathsf{F}_\mathrm{R}^{-1}$ that connects the relaxed material vectors $\mathsf{F}_\mathrm{R}(\delta\boldsymbol{X})$ to the current state of strain given by $\mathsf{F}(\delta\boldsymbol{X})$.

developing constitutive relations. The matrix logarithm provides a mapping from the multiplicative group of deformation gradients to its Lie algebra, which is indeed a linear space suitable to host the description of stresses. This argument can be summarised by saying that the use of mathematical representations of physical quantities must respect their mechanical meaning. The fundamental role of logarithmic strains is to guarantee such consistency.

Within the general setting that we propose, we first specialise our treatment to the basic case in which material parameters are assumed constant. This can of course be relaxed to better represent real fluids. Nevertheless, we can already capture nontrivial qualitative features of viscoelastic flows. We are able to obtain a dependence of rheological curves on the shear rate and even on the flow type without any such dependence in the material parameters. Indeed, those effects turn out to be a result of how the different flows affect the elastic part of the stress, with particular reference to the dynamics of the principal stress directions.

2.1 The constitutive framework

We now start from the decomposition of the Cauchy stress as $\boldsymbol{\sigma} = -p\mathsf{I} + \mathsf{T}_\mathrm{vi} + \mathsf{T}_\mathrm{el}$, introduced above for incompressible materials. In what follows, we assume $\mathsf{T}_\mathrm{vi} = 2\eta\mathsf{D}$, wherein a viscosity $\eta \geq 0$ multiplies the symmetric part of the velocity gradient D. At this stage, we pose no restriction on the possibly nonlinear dependence of η on other kinematic descriptors. In later sections we will consider the simplest case of a constant

viscosity to highlight the role of the elastic term in determining the model rheology.

To propose a relation for the elastic stress $\mathsf{T}_{\rm el}$ we need to introduce a tensorial description of the local state of deformation in which no elastic response would be present. Recall that the placement $\boldsymbol{\varphi}$ maps the label $\boldsymbol{X}$ of a material point into its position $\boldsymbol{\varphi}(\boldsymbol{X},t)$ in space at time t. Its gradient F, that represents derivatives of a position in space with respect to material labels, acts as a linear transformation on vectors in the material manifold, mapping them into vectors in the ambient space (see Figure 2.1, top).

In purely elastic theories, the relaxed state is most often assumed to be realized by a reference material configuration corresponding to the set of labels $\boldsymbol{X}$. We are interested in a more general situation and then we introduce the tensor field $\mathsf{F}_{\rm R}$, that maps the reference material line elements $\delta\boldsymbol{X}$ into elastically relaxed material line elements. Notice that $\mathsf{F}_{\rm R}$ need not be the gradient of any deformation: it is a local description of how the material would like to be strained to relax elastic stresses. As a consequence, these stresses will depend upon the mapping $\mathsf{F}_{\rm el} := \mathsf{F}\mathsf{F}_{\rm R}^{-1}$ that connects the relaxed material vectors $\mathsf{F}_{\rm R}(\delta\boldsymbol{X})$ to the current state of strain given by $\mathsf{F}(\delta\boldsymbol{X})$ (see Figure 2.1, bottom).

Following this construction of the elastic deformation gradient, we obtain the right and left Cauchy–Green tensors $\mathsf{C}_{\rm el} := \mathsf{F}_{\rm el}^{\mathsf{T}}\mathsf{F}_{\rm el}$ and $\mathsf{B}_{\rm el} := \mathsf{F}_{\rm el}\mathsf{F}_{\rm el}^{\mathsf{T}}$, respectively, sometimes referred to as elastic strain tensors. Both quantities are objective: $\mathsf{B}_{\rm el}$ is covariant as $\boldsymbol{\sigma}$ should be, while $\mathsf{C}_{\rm el}$ is frame-invariant, as is $\mathsf{F}_{\rm R}$, given that relaxed line elements are still material ones and are not affected by changes in the spatial frame of reference. By introducing the constant elastic modulus $\kappa \geq 0$, we can then postulate

$$\mathsf{T}_{\rm el} = \kappa \log \mathsf{B}_{\rm el} = \kappa \log(\mathsf{F}\mathsf{F}_{\rm R}^{-1}\mathsf{F}_{\rm R}^{-\mathsf{T}}\mathsf{F}^{\mathsf{T}}). \tag{2.1}$$

We stress the fact that, by using $\mathsf{B}_{\rm el}$ in the definition of the stress, we make sure that no elastic response arises when the relative deformation between F and $\mathsf{F}_{\rm R}$ is just a rigid rotation. Moreover, the fact that for incompressible motions we have $\det\mathsf{F} = \det\mathsf{F}_{\rm R} = 1$ implies that $\det\mathsf{B}_{\rm el} = 1$ and so $\operatorname{tr}\mathsf{T}_{\rm el} = \kappa \operatorname{tr}\log\mathsf{B}_{\rm el} = 0$, as is desirable for a term entering the extra stress. The definition of $\mathsf{F}_{\rm el}$ given above corresponds to the multiplicative decomposition of the deformation gradient as $\mathsf{F} = \mathsf{F}_{\rm el}\mathsf{F}_{\rm R}$, which is part of the standard approach to solid plasticity [45]. Such a decomposition was introduced by Kröner [46] and independently by Lee & Liu [47, 48] and has since proved to be a key tool also in the description of growth and remodelling [49], morphogenesis [50], and active materials [51].

In viscoelastic materials, the microscopic arrangement of molecules determines the state at which the system would converge in the absence of applied forces. This state can evolve in time as a result of deformations and stresses. We thus need to postulate a suitable evolution equation for $\mathsf{F}_{\rm R}$, in keeping with what is customarily done in plasticity theory [45]. Such an equation should imply that, if we keep the material in a static configuration in which some elastic stress is active, then $\mathsf{F}_{\rm R}$ converges exponentially to F with a characteristic time-scale $\tau_{\rm r} \geq 0$ and the elastic stress relaxes to zero. We propose a model based on the following considerations. The rate $(\mathcal{D}_{\boldsymbol{u}}\mathsf{F}_{\rm R})\mathsf{F}_{\rm R}^{-1}$ is a frame-invariant quantity and it belongs to the Lie algebra associated with the group of positive-determinant linear transformations of material line elements into material line elements. Moreover, it must be traceless to preserve the determinant of $\mathsf{F}_{\rm R}$ during the evolution and, finally, it

should vanish whenever the relative deformation between F and F_R is a rotation, namely when there is no elastic strain. A quantity that satisfies all of these requirements is $\log \mathsf{C}_\mathrm{el}$ and we thus postulate that

$$\mathcal{D}_{\boldsymbol{u}} \mathsf{F}_\mathrm{R} = \frac{1}{2\tau_\mathrm{r}} \log(\mathsf{C}_\mathrm{el}) \mathsf{F}_\mathrm{R}. \tag{2.2}$$

The factor of 2 in front of τ_r comes from the fact that $\log \mathsf{C}_\mathrm{el}$ contains twice the elastic strain of the material and it is what we need to have the stress relax as e^{-t/τ_r} in static experiments. As is the case for η, the relaxation time τ_r can depend on other quantities that describe the state of the material provided that it remains frame-invariant.

In summary, the evolution equations of the present model are (1.27), (2.2), and the linear momentum balance

$$\rho \mathcal{D}_{\boldsymbol{u}} \boldsymbol{u} = -\nabla p + \operatorname{div}(2\eta \mathsf{D} + \kappa \log \mathsf{B}_\mathrm{el}). \tag{2.3}$$

Boundary conditions must be specified only for the velocity field $\boldsymbol{u}$, while initial conditions are also needed for F and F_R.

2.1.1 Evolution of the elastic strain and energy balance

The tensorial measure of elastic strain provided by B_el satisfies an evolution equation that is determined by those of F and F_R. Remembering equations (1.27) and (2.2), we get

$$\mathsf{O} = \mathcal{D}_{\boldsymbol{u}}(\mathsf{F}^{-1}\mathsf{F}) = (\mathcal{D}_{\boldsymbol{u}}\mathsf{F}^{-1})\mathsf{F} + \mathsf{F}^{-1}(\mathcal{D}_{\boldsymbol{u}}\mathsf{F}),$$

from which

$$\mathcal{D}_{\boldsymbol{u}}\mathsf{F}^{-1} = -\mathsf{F}^{-1}(\mathcal{D}_{\boldsymbol{u}}\mathsf{F})\mathsf{F}^{-1} = -\mathsf{F}^{-1}\nabla\boldsymbol{u} \qquad \text{and} \qquad \mathcal{D}_{\boldsymbol{u}}\mathsf{F}^{-\mathsf{T}} = -\nabla\boldsymbol{u}^{\mathsf{T}}\mathsf{F}^{-\mathsf{T}},$$

and

$$\mathsf{O} = \mathcal{D}_{\boldsymbol{u}}(\mathsf{F}_\mathrm{R}^{-1}\mathsf{F}_\mathrm{R}) = (\mathcal{D}_{\boldsymbol{u}}\mathsf{F}_\mathrm{R}^{-1})\mathsf{F}_\mathrm{R} + \mathsf{F}_\mathrm{R}^{-1}(\mathcal{D}_{\boldsymbol{u}}\mathsf{F}_\mathrm{R}),$$

from which

$$\mathcal{D}_{\boldsymbol{u}}\mathsf{F}_\mathrm{R}^{-1} = -\mathsf{F}_\mathrm{R}^{-1}(\mathcal{D}_{\boldsymbol{u}}\mathsf{F}_\mathrm{R})\mathsf{F}_\mathrm{R}^{-1} = -\frac{1}{2\tau_\mathrm{r}}\mathsf{F}_\mathrm{R}^{-1}\log(\mathsf{C}_\mathrm{el}) \qquad \text{and} \qquad \mathcal{D}_{\boldsymbol{u}}\mathsf{F}_\mathrm{R}^{-\mathsf{T}} = -\frac{1}{2\tau_\mathrm{r}}\log(\mathsf{C}_\mathrm{el})\mathsf{F}_\mathrm{R}^{-\mathsf{T}}.$$

With these results we can easily compute

$$\mathcal{D}_{\boldsymbol{u}}\mathsf{B}_\mathrm{el} = \mathcal{D}_{\boldsymbol{u}}(\mathsf{F}\mathsf{F}_\mathrm{R}^{-1}\mathsf{F}_\mathrm{R}^{-\mathsf{T}}\mathsf{F}^{\mathsf{T}}) = \nabla\boldsymbol{u}\mathsf{B}_\mathrm{el} + \mathsf{B}_\mathrm{el}\nabla\boldsymbol{u}^{\mathsf{T}} - \frac{1}{\tau_\mathrm{r}}\mathsf{F}\mathsf{F}_\mathrm{R}^{-1}(\log \mathsf{C}_\mathrm{el})\mathsf{F}_\mathrm{R}^{-\mathsf{T}}\mathsf{F}^{\mathsf{T}}. \tag{2.4}$$

By applying the polar decomposition, we define the orthogonal tensor R_el via the identity $\mathsf{F}\mathsf{F}_\mathrm{R}^{-1} = \mathsf{B}_\mathrm{el}^{\frac{1}{2}}\mathsf{R}_\mathrm{el}$. Moreover, any analytic function f of the tensors C_el and B_el is such that $f(\mathsf{B}_\mathrm{el}) = \mathsf{R}_\mathrm{el} f(\mathsf{C}_\mathrm{el})\mathsf{R}_\mathrm{el}^{-1}$, entailing the identity

$$\mathsf{F}\mathsf{F}_\mathrm{R}^{-1}(\log \mathsf{C}_\mathrm{el})\mathsf{F}_\mathrm{R}^{-\mathsf{T}}\mathsf{F}^{\mathsf{T}} = \mathsf{B}_\mathrm{el}^{\frac{1}{2}}(\log \mathsf{B}_\mathrm{el})\mathsf{B}_\mathrm{el}^{\frac{1}{2}} = \mathsf{B}_\mathrm{el}\log \mathsf{B}_\mathrm{el}. \tag{2.5}$$

Substituting (2.5) into (2.4), we finally obtain

$$\mathcal{D}_{\boldsymbol{u}}\mathsf{B}_{\mathrm{el}} = \nabla\boldsymbol{u}\mathsf{B}_{\mathrm{el}} + \mathsf{B}_{\mathrm{el}}\nabla\boldsymbol{u}^{\mathsf{T}} - \frac{1}{\tau_{\mathrm{r}}}\mathsf{B}_{\mathrm{el}}\log\mathsf{B}_{\mathrm{el}}. \tag{2.6}$$

We stress that the first two terms on the right-hand side of (2.6) are of a kinematic nature, since they descend directly from the definition of B_{el} and equation (1.27). Together with the material derivative they constitute a specific objective rate, the upper-convected one, which is not postulated but is rather a consequence of basic kinematics. In Oldroyd's approach other objective rates, such as the lower-convected derivative, are equally valid. We can expect those to be relevant in constitutive theories in which the evolution of F_{R} is different and could produce additional terms in the evolution equations for B_{el}. Indeed, the last term of (2.6) depends on the constitutive choice we made about the dynamics of F_{R}, intimately linked to the form of the elastic stress as well. The form of equation (2.6) remains unchanged if τ_{r} depends on other kinematic quantities because the first derivatives of B_{el} are expressed in terms of the first derivatives of F_{R}, proportional to $1/\tau_{\mathrm{r}}$, and no higher-order derivatives are involved. Lastly, if $\det\mathsf{B}_{\mathrm{el}} = 1$ at the initial time, then it remains such for all times, because $\mathrm{tr}(\nabla\boldsymbol{u}) = 0 = \mathrm{tr}(\log\mathsf{B}_{\mathrm{el}})$.

Equation (2.6) contains in itself less information than the coupled system of (1.27) and (2.2) but it offers a more direct way to compare our framework with established approaches. In Oldroyd-type models, an evolution for the extra stress or for the elastic stress is postulated. To make a comparison we look for an evolution equation involving $\mathsf{T}_{\mathrm{el}} = \kappa\log\mathsf{B}_{\mathrm{el}}$ by multiplying equation (2.6) by $\kappa\mathsf{B}_{\mathrm{el}}^{-1}$. Nevertheless, in general we have that $\mathcal{D}_{\boldsymbol{u}}(\log\mathsf{B}_{\mathrm{el}})$ differs from $\mathsf{B}_{\mathrm{el}}^{-1}\mathcal{D}_{\boldsymbol{u}}\mathsf{B}_{\mathrm{el}}$, due to the tensorial nature of B_{el}, and B_{el} does not often commute with $\nabla\boldsymbol{u}$. It is only when $\nabla\boldsymbol{u}$ and B_{el} are both diagonal on the same *time-independent* basis that we can obtain precisely $\mathcal{D}_{\boldsymbol{u}}\mathsf{T}_{\mathrm{el}} = 2\kappa\mathsf{D} - \mathsf{T}_{\mathrm{el}}/\tau_{\mathrm{r}}$. This shows that in extensional flows we will get results akin to those of the simplest Maxwell model (albeit with a separate viscous contribution). Such a simplification is never true in simple shear or generic flows. A general translation of (2.6) would rather be

$$\mathcal{D}_{\boldsymbol{u}}\big(e^{\mathsf{T}_{\mathrm{el}}/\kappa}\big) = \nabla\boldsymbol{u}\,e^{\mathsf{T}_{\mathrm{el}}/\kappa} + e^{\mathsf{T}_{\mathrm{el}}/\kappa}\nabla\boldsymbol{u}^{\mathsf{T}} - \frac{1}{\kappa\tau_{\mathrm{r}}}e^{\mathsf{T}_{\mathrm{el}}/\kappa}\mathsf{T}_{\mathrm{el}}, \tag{2.7}$$

which shows a significant structural difference compared to Oldroyd-like models. Even considering formulations that employ conformation tensors [14] or log-conformation tensors [52], one would essentially find the same difference. In fact, $\mathsf{T}_{\mathrm{el}}/\kappa$ would be the candidate conformation tensor and we clearly see its exponential appearing in (2.7) at places where standard models would put $\mathsf{T}_{\mathrm{el}}/\kappa$.

It is somewhat surprising that the arguments—quite natural from the solid mechanics perspective—that lead to the definition of our framework imply such a dramatic modification when contrasted with Oldroyd's approach. The reasons to embrace such a change are deeply rooted in the proper mathematical representation of mechanical quantities. Stresses must belong to a linear space, while the dynamics of kinematic quantities such as F, F_{R}, and B_{el}, that are quite natural choices to describe the state of the deformation, takes place on tensorial manifolds. Moreover, the evolution of the stress tensor should be a consequence of the evolution of kinematic quantities and constitutive laws.

On the other hand, in the linearised limit of small elastic stresses and strains, we may expect to recover some classical model starting from equation (2.7). Indeed, when $\|\mathsf{T}_{\mathrm{el}}/\kappa\| = \|\log \mathsf{B}_{\mathrm{el}}\| \ll 1$, we can use the approximation $\exp(\mathsf{T}_{\mathrm{el}}/\kappa) \approx \mathsf{I} + \mathsf{T}_{\mathrm{el}}/\kappa$ and substitute it into (2.7) to obtain

$$\mathcal{D}_{\boldsymbol{u}}(\mathsf{I} + \mathsf{T}_{\mathrm{el}}/\kappa) = \nabla \boldsymbol{u}\,(\mathsf{I} + \mathsf{T}_{\mathrm{el}}/\kappa) + (\mathsf{I} + \mathsf{T}_{\mathrm{el}}/\kappa)\nabla \boldsymbol{u}^{\mathsf{T}} - \frac{1}{\kappa\tau_{\mathrm{r}}}(\mathsf{I} + \mathsf{T}_{\mathrm{el}}/\kappa)\mathsf{T}_{\mathrm{el}}, \tag{2.8}$$

that gives, in the case of constant κ and τ_{r}, the linearised equation

$$\mathsf{T}_{\mathrm{el}} + \tau_{\mathrm{r}}(\mathcal{D}_{\boldsymbol{u}}\mathsf{T}_{\mathrm{el}} - \nabla \boldsymbol{u}\,\mathsf{T}_{\mathrm{el}} - \mathsf{T}_{\mathrm{el}}\nabla \boldsymbol{u}^{\mathsf{T}}) = 2\kappa\tau_{\mathrm{r}}\mathsf{D}. \tag{2.9}$$

Equation (2.9) corresponds to the upper-convected Maxwell model with relaxation time τ_{r} and viscosity $\eta_0 = \kappa\tau_{\mathrm{r}}$. This shows that our model is a proper generalisation of Maxwell's model to the case of finite elastic strains. Furthermore, retaining the last term of equation (2.8), which is quadratic in T_{el}, we find the Giesekus model [39] with a specific choice of material parameters.

It is finally instructive to compute the energy balance implied by our model. For a smooth divergence-free velocity field $\boldsymbol{u}$ that satisfies homogeneous boundary conditions in a domain Ω, we can multiply equation (2.3) by $\boldsymbol{u}$ and integrate by parts to obtain

$$\begin{aligned}\frac{d}{dt}\bigg(\int_\Omega \frac{\rho}{2}|\boldsymbol{u}|^2\,d\boldsymbol{x}\bigg) &= \int_\Omega p\,\mathrm{div}\,\boldsymbol{u}\,d\boldsymbol{x} - \int_\Omega (2\eta\mathsf{D} + \kappa\log\mathsf{B}_{\mathrm{el}}) : \nabla\boldsymbol{u}\,d\boldsymbol{x} \\ &= -\int_\Omega 2\eta|\mathsf{D}|^2\,d\boldsymbol{x} - \int_\Omega \kappa\log\mathsf{B}_{\mathrm{el}} : \mathsf{D}\,d\boldsymbol{x}, \end{aligned}\tag{2.10}$$

where we used the matrix scalar product $\mathsf{A} : \mathsf{C} := \mathrm{tr}(\mathsf{A}^{\mathsf{T}}\mathsf{C})$, with respect to which symmetric and antisymmetric tensors are orthogonal, and the notation $|\mathsf{A}|^2 = \mathsf{A} : \mathsf{A}$. Then we can reconstruct the time derivative of the stored elastic energy by multiplying equation (2.6) by $(\kappa/2)\mathsf{B}_{\mathrm{el}}^{-1}\log\mathsf{B}_{\mathrm{el}}$, which leads to

$$\frac{d}{dt}\bigg(\int_\Omega \frac{\kappa}{4}|\log\mathsf{B}_{\mathrm{el}}|^2\,d\boldsymbol{x}\bigg) = \int_\Omega \kappa\log\mathsf{B}_{\mathrm{el}} : \mathsf{D}\,d\boldsymbol{x} - \int_\Omega \frac{\kappa}{2\tau_{\mathrm{r}}}|\log\mathsf{B}_{\mathrm{el}}|^2\,d\boldsymbol{x}. \tag{2.11}$$

By taking the sum of (2.10) and (2.11), we find

$$\frac{d}{dt}\bigg(\int_\Omega \frac{\rho}{2}|\boldsymbol{u}|^2\,d\boldsymbol{x} + \int_\Omega \frac{\kappa}{4}|\log\mathsf{B}_{\mathrm{el}}|^2\,d\boldsymbol{x}\bigg) = -\int_\Omega 2\eta|\mathsf{D}|^2\,d\boldsymbol{x} - \int_\Omega \frac{\kappa}{2\tau_{\mathrm{r}}}|\log\mathsf{B}_{\mathrm{el}}|^2\,d\boldsymbol{x} \le 0, \tag{2.12}$$

showing that the total energy, sum of kinetic and elastic contributions, cannot increase in time and it is lowered via either viscous dissipation, proportional to $|\mathsf{D}|^2$, or plastic dissipation, proportional to $|\log\mathsf{B}_{\mathrm{el}}|^2$. This proves that the class of models we introduced in the previous section is thermodynamically consistent. It is worth noticing that the cancellation of the exchange term occurring when we sum the two equations stems from the perfect balance between the elastic stress and the plastic evolution of F_{R}.

2.2 Small-amplitude oscillatory flows

To investigate the viscoelastic behavior of the constitutive model introduced in Section 2.1 under the simplest assumption of constant η and τ_r, we should first analyze its prediction in small-amplitude oscillatory shear (SAOS) experiments. From the discussion in the previous section, we clearly expect to find linear viscoelastic properties that coincide with those of an upper-convected Maxwell model. Nevertheless, we find it useful to explicitly show this computation to identify the role of each parameter. With our model, the evolution equation for F_R in oscillatory shear cannot be easily solved in an analytical way. Nevertheless, we can appeal to the fact that, due to the linearization implied in the small-amplitude analysis, the results obtained in simple shear are equivalent to those obtained from a small-amplitude oscillatory extensional flow, up to a 45-degree rotation of coordinates. In fact, the deformation map in shear and extension are, respectively,

$$\boldsymbol{\varphi}_\mathrm{sh}(t,x,y) = \begin{pmatrix} x+\gamma(t;\omega,\gamma_0)y \\ y \end{pmatrix} \quad \text{and} \quad \boldsymbol{\varphi}_\mathrm{ex}(t,x,y) = \begin{pmatrix} e^{\frac{1}{2}\gamma(t;\omega,\gamma_0)}x \\ e^{-\frac{1}{2}\gamma(t;\omega,\gamma_0)}y \end{pmatrix},$$

where the strain is given by $\gamma(t;\omega,\gamma_0) = \gamma_0 \sin(\omega t)$, with γ_0 representing the maximum strain amplitude. The corresponding rate of deformation tensors, connected by a 45-degree rotation, are

$$\mathsf{D}_\mathrm{sh} = \begin{pmatrix} 0 & \dot\gamma/2 \\ \dot\gamma/2 & 0 \end{pmatrix} \quad \text{and} \quad \mathsf{D}_\mathrm{ex} = \begin{pmatrix} \dot\gamma/2 & 0 \\ 0 & -\dot\gamma/2 \end{pmatrix},$$

and a similar relation holds between the linearized Cauchy–Green tensors, that read

$$\mathsf{F}_\mathrm{sh}\mathsf{F}_\mathrm{sh}^\mathsf{T} \approx \begin{pmatrix} 1 & \gamma \\ \gamma & 1 \end{pmatrix} \quad \text{and} \quad \mathsf{F}_\mathrm{ex}\mathsf{F}_\mathrm{ex}^\mathsf{T} \approx \begin{pmatrix} 1+\gamma & 0 \\ 0 & 1-\gamma \end{pmatrix}.$$

We can then restrict attention to the extensional flow case, setting

$$\mathsf{F}(t;\omega,\gamma_0) = \mathsf{F}_\mathrm{ex} = \begin{pmatrix} e^{\gamma(t)/2} & 0 \\ 0 & e^{-\gamma(t)/2} \end{pmatrix} \quad \text{and assuming} \quad \mathsf{F}_\mathrm{R}(t) = \begin{pmatrix} e^{\gamma_\mathrm{R}(t)/2} & 0 \\ 0 & e^{-\gamma_\mathrm{R}(t)/2} \end{pmatrix}.$$

Under these provisions, the evolution equation for F_R reduces to the scalar evolution equation

$$\frac{\partial \gamma_\mathrm{R}}{\partial t} = \frac{1}{\tau_\mathrm{r}}(\gamma_0 \sin(\omega t) - \gamma_\mathrm{R}), \tag{2.13}$$

that, assuming the initial condition $\gamma_\mathrm{R}(0) = 0$, leads to

$$\gamma_\mathrm{R}(t) = \frac{\gamma_0 \omega \tau_\mathrm{r}}{1+\omega^2\tau_\mathrm{r}^2} e^{-t/\tau_\mathrm{r}} + \frac{\gamma_0[\sin(\omega t) - \omega\tau_\mathrm{r}\cos(\omega t)]}{1+\omega^2\tau_\mathrm{r}^2},$$

which, for sufficiently large times $t \gg \tau_\mathrm{r}$, reduces to

$$\gamma_\mathrm{R}(t) \approx \gamma_0 \frac{\sin(\omega t) - \omega\tau_\mathrm{r}\cos(\omega t)}{1+\omega^2\tau_\mathrm{r}^2}. \tag{2.14}$$

Regarding the elastic strain tensors, we find

$$\mathsf{B}_{\mathrm{el}} = \mathsf{C}_{\mathrm{el}} = \begin{pmatrix} e^{\gamma-\gamma_{\mathrm{R}}} & 0 \\ 0 & e^{-(\gamma-\gamma_{\mathrm{R}})} \end{pmatrix}$$

and the elastic stress becomes

$$\mathsf{T}_{\mathrm{el}}(t;\omega,\gamma_0,\tau_{\mathrm{r}},\kappa) = \kappa \log \mathsf{B}_{\mathrm{el}} = \kappa(\gamma-\gamma_{\mathrm{R}}) \begin{pmatrix} 1 & 0 \\ 0 & -1 \end{pmatrix},$$

while the deformation rate tensor is

$$\mathsf{D}(t;\omega,\gamma_0) = \frac{\gamma_0\omega}{2}\cos(\omega t)\hat{\mathsf{D}}, \quad \text{with} \quad \hat{\mathsf{D}} := \begin{pmatrix} 1 & 0 \\ 0 & -1 \end{pmatrix}.$$

We can then compute the time-dependent projection

$$\begin{aligned} \zeta(t;\omega,\gamma_0,\tau_{\mathrm{r}},\kappa,\eta) &:= \frac{(\mathsf{T}_{\mathrm{el}}+\mathsf{T}_{\mathrm{vi}}):\hat{\mathsf{D}}}{\hat{\mathsf{D}}:\hat{\mathsf{D}}} = \kappa(\gamma-\gamma_{\mathrm{R}}) + \eta\gamma_0\omega\cos(\omega t) \\ &\overset{t\gg\tau_{\mathrm{r}}}{\approx} \gamma_0\kappa\left[\frac{\omega^2\tau_{\mathrm{r}}^2}{1+\omega^2\tau_{\mathrm{r}}^2}\sin(\omega t) + \frac{\omega\tau_{\mathrm{r}}}{1+\omega^2\tau_{\mathrm{r}}^2}\cos(\omega t)\right] + \gamma_0\eta\omega\cos(\omega t) \end{aligned} \tag{2.15}$$

which characterizes the material response in this geometry.

The standard material functions for SAOS experiments are η', η'', G', G'' defined by

$$G'\sin(\omega t) + G''\cos(\omega t) = \omega\eta'\cos(\omega t) + \omega\eta''\sin(\omega t) = \zeta/\gamma_0. \tag{2.16}$$

For our model we thus find

$$G'(\omega;\tau_{\mathrm{r}},\kappa) = \omega\eta''(\omega;\tau_{\mathrm{r}},\kappa) = \omega\frac{\kappa\omega\tau_{\mathrm{r}}^2}{1+\omega^2\tau_{\mathrm{r}}^2}, \tag{2.17}$$

$$G''(\omega;\tau_{\mathrm{r}},\kappa,\eta) = \omega\eta'(\omega;\tau_{\mathrm{r}},\kappa,\eta) = \omega\frac{\kappa\tau_{\mathrm{r}}}{1+\omega^2\tau_{\mathrm{r}}^2} + \omega\eta. \tag{2.18}$$

When η is negligible compared to $\kappa\tau_{\mathrm{r}}$, that is we measure a purely plastic dissipation, the material functions η' and η'' become identical to those predicted by an upper-convected Maxwell model with zero-rate viscosity $\eta_0 = \kappa\tau_{\mathrm{r}}$ (see Figure 2.2). If η is smaller than $\kappa\tau_{\mathrm{r}}$, but not negligible, we obtain a high-frequency plateau in η', that does not appear in η''. This is compatible with experimentally observed behaviour that may be fitted by means of Giesekus models (compare, for instance, our Figure 2.2 with Figures 3.4-4 and 3.4-5 of [13]). In the linear regime, several models collapse on the Oldroyd-B result

$$G'(\omega) = G\frac{(\lambda\omega)^2}{1+(\lambda\omega)^2} \quad \text{and} \quad G''(\omega) = G\frac{\lambda\omega}{1+(\lambda\omega)^2} + \omega\eta_{\mathrm{s}},$$

where G is the high-frequency storage modulus, λ the relaxation time, and η_{s} the high-frequency viscosity. This is the case for the Johnson–Segalman [3], single-mode Phan-Thien–Tanner [10], and Giesekus [39] models and, manifestly, for the constant-parameter

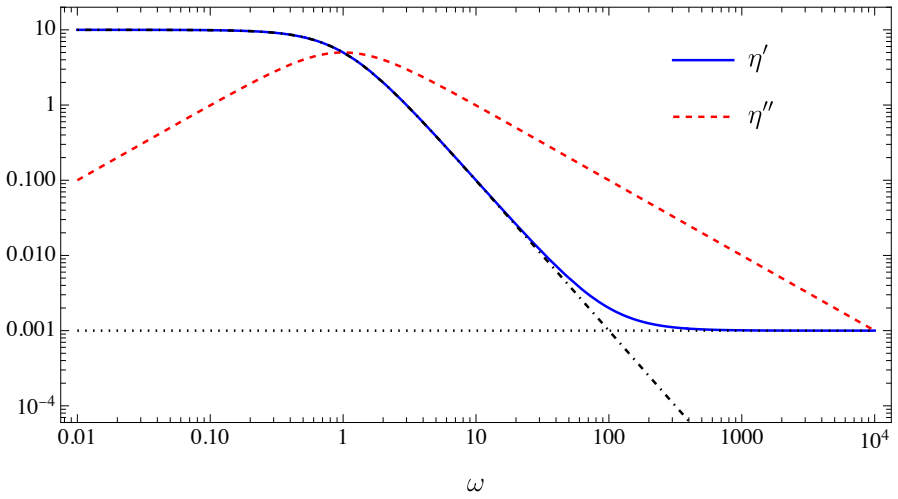

Figure 2.2: *The dependence on the angular frequency ω of the linear viscoelastic moduli η' and η'' of the present model is typical of systems with a single relaxation time.* The dissipative modulus η' is the sum of a plastic contribution (dot-dashed line), identical to the prediction of an upper-convected Maxwell model, and a constant viscous term (dotted line) given by η. The elastic modulus η'' grows linearly, displays the expected peak around $\omega = 1/\tau_r$, and then decays as $1/\omega$. In this example, we chose $\tau_r = 1$ s, $\kappa = 10$ Pa, and $\eta = 10^{-3}$ Pa s.

version of our model with the identifications $G = \kappa$, $\lambda = \tau_r$, and $\eta_s = \eta$. Notably, those models feature other parameters that do not affect the linear regime, while our model has the same number of parameters as the Oldroyd-B model.

The interpretation of the ω-dependence of the dissipative modulus η' is the following: when oscillations are slow, F_R has enough time to evolve and we measure a significant plastic dissipation; when oscillations are fast, F_R remains effectively fixed and the material behaves like a viscoelastic solid, where the measured dissipation is purely viscous. Regarding the elastic response, it is easier to interpret the behaviour of $G' = \omega\eta''$: if the relaxation time τ_r is much shorter than $1/\omega$, then the elastic response is negligible and $G' \propto \omega^2\tau_r^2$; when $\tau_r \gg 1/\omega$, then F_R remains effectively fixed and $G' \approx \kappa$ is independent of ω. Hence, with a sufficiently broad range of frequency, oscillatory flow experiments would allow to measure all of the material parameters.

2.3 Stress growth after inception of steady flows

In this section, we analyze the evolution of the stress when a steady flow is suddenly imposed starting from a stress-free static condition. The constant strain rate is $\dot\gamma := \sqrt{2\mathsf{D} : \mathsf{D}}$. The components of the extra stress are represented by the following time-

dependent material coefficients

$$\eta^+_{\text{eff}}(t;\tau_{\text{r}},\kappa,\eta,\dot\gamma) := \frac{1}{\dot\gamma}\frac{\mathsf{T}:\hat{\mathsf{D}}}{\hat{\mathsf{D}}:\hat{\mathsf{D}}} \qquad \text{and} \qquad \Psi^+_{\text{eff}}(t;\tau_{\text{r}},\kappa,\eta,\dot\gamma) := \frac{2}{\dot\gamma^2}\frac{\mathsf{T}:\hat{\mathsf{G}}}{\hat{\mathsf{G}}:\hat{\mathsf{G}}}, \tag{2.19}$$

where

$$\hat{\mathsf{D}} := \frac{2}{\dot\gamma}\mathsf{D} \quad \text{and} \quad \hat{\mathsf{G}} := \frac{1}{2}(\mathsf{A}\hat{\mathsf{D}} - \hat{\mathsf{D}}\mathsf{A}), \quad \text{having set } \mathsf{A} := \begin{pmatrix} 0 & 1 \\ -1 & 0 \end{pmatrix} \text{ for planar flows.}$$

Following Giusteri & Seto [53], we employ a definition of the material coefficients that is independent of the flow type, to be able to directly compare the results obtained in extensional and simple shear flows.

The definitions given in (2.19) coincide with the standard material functions (viscosity and first normal stress coefficient) in simple shear flows, but can be used to analyze any steady flow. Steady-state material functions will be determined as the long-time limit of η^+_{eff} and Ψ^+_{eff}. We will find analytical expressions in planar and uniaxial extensional flows and then numerically study the case of simple shear.

As a reference for the effects that we wish to capture, we consider rheological features of polymeric solutions such as those reported in [13, Chap. 3.4–3.5]. In particular, we will clearly see differences and similarities between shear and extensional rheology and show how basic phenomena in unsteady as well as steady flows are qualitatively reproduced by the simplest version of our model.

2.3.1 Planar extensional flow

In this case, the deformation map $\boldsymbol{\varphi}$, the deformation gradient F, and the relaxed state F_{R} are given by

$$\boldsymbol{\varphi}(t,x,y) = \begin{pmatrix} e^{\frac{1}{2}\dot\gamma t}x \\ e^{-\frac{1}{2}\dot\gamma t}y \end{pmatrix}, \qquad \mathsf{F} = \begin{pmatrix} e^{\frac{1}{2}\dot\gamma t} & 0 \\ 0 & e^{-\frac{1}{2}\dot\gamma t} \end{pmatrix}, \qquad \mathsf{F}_{\text{R}} = \begin{pmatrix} e^{\frac{1}{2}\gamma_{\text{R}}(t)} & 0 \\ 0 & e^{-\frac{1}{2}\gamma_{\text{R}}(t)} \end{pmatrix}.$$

The evolution equation for F_{R} reduces to the scalar equation

$$\frac{\partial\gamma_{\text{R}}}{\partial t} = \frac{1}{\tau_{\text{r}}}(\dot\gamma t - \gamma_{\text{R}}), \tag{2.20}$$

that, assuming the initial condition $\gamma_{\text{R}}(0) = 0$, leads to

$$\gamma_{\text{R}}(t) = \dot\gamma\left(t - \tau_{\text{r}} + \tau_{\text{r}}e^{-t/\tau_{\text{r}}}\right). \tag{2.21}$$

From this, we easily obtain

$$\log\mathsf{B}_{\text{el}} = \tau_{\text{r}}\dot\gamma\left(1 - e^{-t/\tau_{\text{r}}}\right)\begin{pmatrix} 1 & 0 \\ 0 & -1 \end{pmatrix}. \tag{2.22}$$

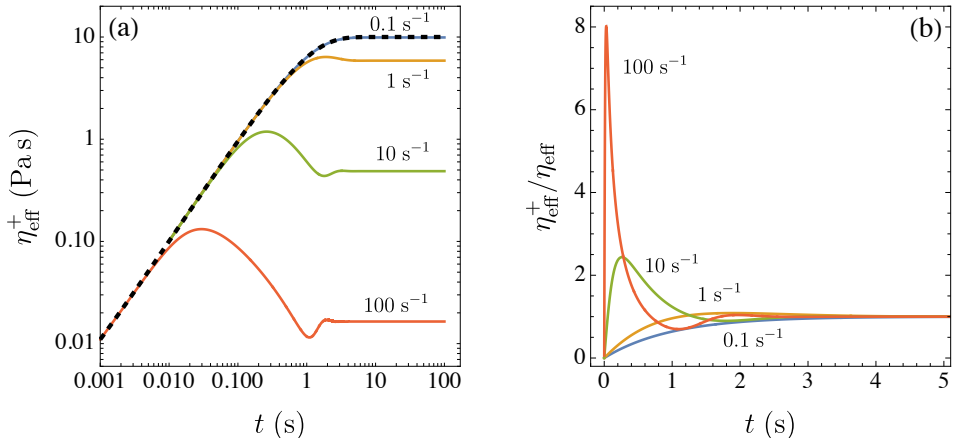

Figure 2.3: *Stress overshoot after inception of steady shear is predicted together with a rate-dependent behavior.* Looking at the time-evolution of $\eta^+_{\rm eff}$ for different values of the shear rate $\dot\gamma$ (curve labels), we see that in the low-rate regime, with $\dot\gamma \ll 1/\tau_{\rm r}$, the rate-dependence becomes negligible and $\eta^+_{\rm eff}$ converges to the extensional flow result (black dashed line in panel (a)). At high shear rates, $\dot\gamma \gtrsim 1/\tau_{\rm r}$, the growth of $\eta^+_{\rm eff}$ is hindered, it reaches a maximum at a strain $\dot\gamma t \approx 3$, and then decays toward a rate-dependent asymptotic value, with possibly a few oscillations. This behavior is even clearer by looking at the data normalized, in panel (b), by the steady value $\eta_{\rm eff}$. The values of material parameters are $\tau_{\rm r} = 1$ s, $\kappa = 10$ Pa, and $\eta = 10^{-3}$ Pa s.

Recalling that in this case the deformation rate tensor is

$$\mathsf{D} = \frac{\dot\gamma}{2}\begin{pmatrix} 1 & 0 \\ 0 & -1 \end{pmatrix},$$

we find

$$\eta^+_{\rm eff}(t;\tau_{\rm r},\kappa,\eta,\dot\gamma) = \kappa\tau_{\rm r}\left(1 - e^{-t/\tau_{\rm r}}\right) + \eta \qquad \text{and} \qquad \Psi^+_{\rm eff}(t;\tau_{\rm r},\kappa,\eta,\dot\gamma) = 0. \tag{2.23}$$

We stress that $\eta^+_{\rm eff}$ turns out to be independent of the shear rate $\dot\gamma$, and so is the steady-state apparent viscosity

$$\eta_{\rm eff}(\tau_{\rm r},\kappa,\eta) := \lim_{t\to+\infty} \eta^+_{\rm eff}(t;\tau_{\rm r},\kappa,\eta) = \kappa\tau_{\rm r} + \eta,$$

which is also identical to the zero-frequency dissipative modulus $\eta'(0;\tau_{\rm r},\kappa,\eta)$. The normal stress coefficient $\Psi^+_{\rm eff}$ is rate-independent in a trivial way: it is identically zero in extensional flows due to symmetry reasons.

2.3.2 Uniaxial extensional flow

In uniaxial extensional flow the deformation map $\boldsymbol{\varphi}$ is given by

$$\boldsymbol{\varphi}(t,x,y,z) = (e^{-\frac{\dot\gamma t}{4}}x, e^{-\frac{\dot\gamma t}{4}}y, e^{\frac{\dot\gamma t}{2}}z)^{\mathsf{T}},$$

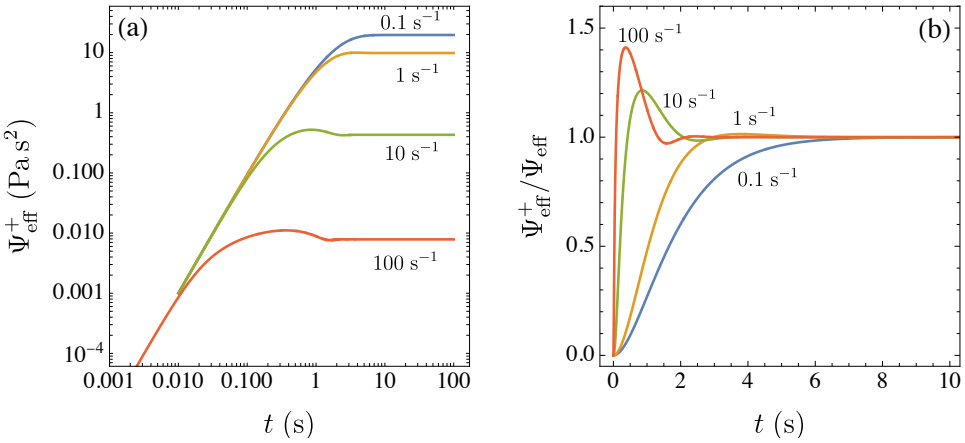

Figure 2.4: *The first normal stress coefficient $\Psi^+_{\rm eff}$ is nonzero in simple shear and its growth after inception of steady shear is rate-dependent.* At low rates ($\dot\gamma << 1/\tau_{\rm r}$) the rate-dependence disappears and the growth is monotonic, while for $\dot\gamma \gtrsim 1/\tau_{\rm r}$ we observe a short-time peak followed by a decay toward the rate-dependent steady value $\Psi_{\rm eff}$ (panel (a)). This behavior is emphasized in the data normalized by the steady value $\Psi_{\rm eff}$, shown in panel (b). The values of material parameters are $\tau_{\rm r} = 1$ s, $\kappa = 10$ Pa, and $\eta = 10^{-3}$ Pa s.

and the deformation gradient F and the relaxed state $\mathsf{F}_{\rm R}$ are given by

$$\mathsf{F} = \begin{pmatrix} e^{-\dot\gamma t/4} & 0 & 0 \\ 0 & e^{-\dot\gamma t/4} & 0 \\ 0 & 0 & e^{\dot\gamma t/2} \end{pmatrix}, \qquad \mathsf{F}_{\rm R} = \begin{pmatrix} e^{-\gamma_{\rm R}/4} & 0 & 0 \\ 0 & e^{-\gamma_{\rm R}/4} & 0 \\ 0 & 0 & e^{\gamma_{\rm R}/2} \end{pmatrix}.$$

The evolution equation for $\mathsf{F}_{\rm R}$ reduces again to (2.20) with solution (2.21). Since we obtain

$$\log \mathsf{B}_{\rm el} = \dot\gamma\tau_{\rm r}\left(1 - e^{-t\tau_{\rm r}}\right)\begin{pmatrix} -1/2 & 0 & 0 \\ 0 & -1/2 & 0 \\ 0 & 0 & 1 \end{pmatrix} \qquad \text{and} \qquad \mathsf{D} = \frac{\dot\gamma}{2}\begin{pmatrix} -1/2 & 0 & 0 \\ 0 & -1/2 & 0 \\ 0 & 0 & 1 \end{pmatrix},$$

we eventually arrive at a result which is identical to the one obtained for planar extensional flows.

2.3.3 Simple shear

For simple shear flows, the deformation map $\boldsymbol{\varphi}$ and the deformation gradient F are given by

$$\boldsymbol{\varphi}(t, x, y, \dot\gamma) = \begin{pmatrix} x + y\dot\gamma t \\ y \end{pmatrix} \qquad \text{and} \qquad \mathsf{F} = \begin{pmatrix} 1 & \dot\gamma t \\ 0 & 1 \end{pmatrix},$$

but there is no reason to assume a specific shape for the relaxed state F_R, which must be determined by solving the evolution equation (2.2). This is a fully tensorial evolution equation that, generally, cannot be reduced to a scalar one. We then solve it numerically.

A very important consequence of the structure of equation (2.2) is that the eigenvectors of B_el rotate over time and are different from those of D. This gives rise to two important effects: the first normal stress coefficient is no longer zero and we observe a dependence of the material functions η^+_eff and Ψ^+_eff on the shear rate $\dot\gamma$. In the low-rate regime, with $\dot\gamma \ll 1/\tau_\mathrm{r}$, the rate-dependence becomes negligible and η^+_eff converges to the extensional flow result (2.23), which is also coincident with the prediction, for simple shear, of an upper-convected Maxwell model (though this would give a different result in extension). When, on the other hand, $\dot\gamma \gtrsim 1/\tau_\mathrm{r}$, the measured shear stress stems from a competition between the speed of the rotation of stress eigenvectors and that of the plastic relaxation. Essentially, the growth of η^+_eff is hindered, it reaches a maximum at a strain $\dot\gamma t \approx 3$, and then decays toward a rate-dependent asymptotic value, with possibly a few oscillations (see Figure 2.3). A similar behavior is followed by the normal stress coefficient Ψ^+_eff that shows a rate-independent growth for $\dot\gamma \ll 1/\tau_\mathrm{r}$ and a rate-dependent asymptotic value for $\dot\gamma \gtrsim 1/\tau_\mathrm{r}$ (see Figure 2.4). Our findings are qualitatively compatible with experimental data as can be seen by comparing them with Figures 3.4-7, 3.4-8, 3.4-9, and 3.4-10 of [13], which are reprinted in the Appendix to this thesis.

The steady state material functions η_eff and Ψ_eff display, in simple shear, a rate-dependent behavior of shear-thinning type (Figure 2.5). The effective viscosity decreases, for $\dot\gamma \gtrsim 1/\tau_\mathrm{r}$, from the low-rate value given by $\kappa\tau_\mathrm{r} + \eta$ to the asymptotic value set by η. We thus see that plastic dissipation dominates the low-rate material response. The effective normal stress coefficient, which is not influenced by the viscosity parameter η, simply decreases from its zero-rate value and vanishes asymptotically. Overall, the simple assumptions present in our model with constant parameters can reproduce qualitative features common to several viscoelastic fluids while providing an understanding of the underlying competition between elasticity, relaxation, and flow geometry that cannot be achieved by means of empirical data-fitting laws.

In this section, we treated simple shear as a two-dimensional flow. If, on the other hand, we view it as a planar but three-dimensional flow, a second normal stress coefficient becomes relevant for the characterization of the material. As long as the deformation remains planar, the present model assigns a vanishing stress in the third spatial direction. This implies that the second normal stress coefficient coincides always with $-\Psi_\mathrm{eff}/2$. The sign of this quantity is consistent with most measurements in the context of viscoelastic fluids, but the reported magnitude is typically significantly lower [54]. We believe that further consideration of how to capture experimental observations of second normal stress coefficients will be an important direction for future investigations.

2.4 Stress relaxation after a sudden deformation

A fundamental parameter of our model is the relaxation time τ_r and it can be directly related to stress relaxation experiments. We consider a material held in a static con-

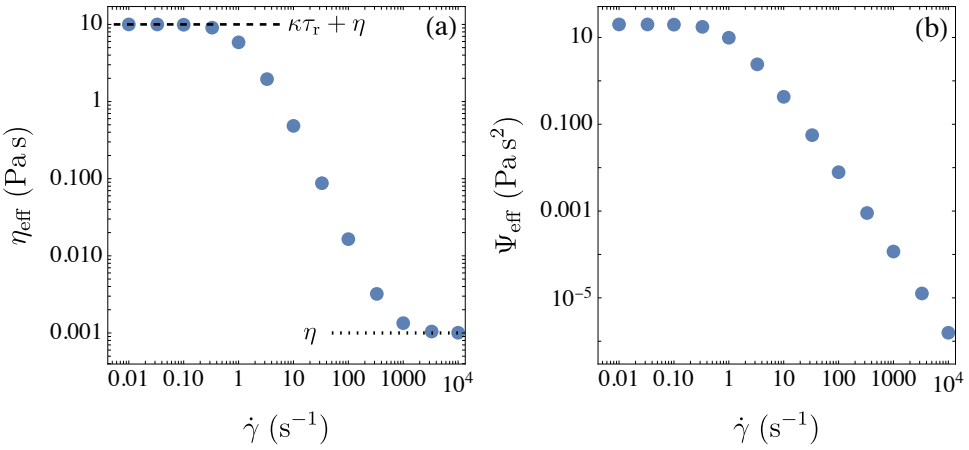

Figure 2.5: *The rate dependence in simple shear of the steady-state material functions η_{eff} and Ψ_{eff} displays a shear-thinning behavior common to many viscoelastic fluids.* The effective viscosity, in panel (a), interpolates between the zero-rate value, given by $\kappa\tau_r + \eta$ (dashed line), and η (dotted line), while the effective normal stress coefficient, in panel (b), simply decreases to zero. The values of material parameters are $\tau_r = 1$ s, $\kappa = 10$ Pa, and $\eta = 10^{-3}$ Pa s.

figuration after a very rapid homogeneous deformation. In the case of an extensional deformation, we can compute the time-dependent elastic stress by taking

$$\mathsf{F} = \begin{pmatrix} e^{\frac{1}{2}\gamma_0} & 0 \\ 0 & e^{-\frac{1}{2}\gamma_0} \end{pmatrix}, \qquad \mathsf{F}_R = \begin{pmatrix} e^{\frac{1}{2}\gamma_R(t)} & 0 \\ 0 & e^{-\frac{1}{2}\gamma_R(t)} \end{pmatrix}.$$

with γ_0 constant. The evolution equation for F_R easily leads to $\gamma_R(t) = \gamma_0(1 - e^{-t/\tau_r})$ and

$$\mathsf{T}_{el} = \kappa \log \mathsf{B}_{el} = (\gamma_0 - \gamma_R) \begin{pmatrix} 1 & 0 \\ 0 & -1 \end{pmatrix} = \kappa\gamma_0 e^{-t/\tau_r} \begin{pmatrix} 1 & 0 \\ 0 & -1 \end{pmatrix}. \tag{2.24}$$

From this, we clearly see that the stress decays exponentially with rate $1/\tau_r$. By numerical integration of the evolution equation for F_R, we obtain the same decay also in the case of a simple shear deformation. Nevertheless, in simple shear the prefactor can depend nonlinearly on γ_0 for large initial strain. At this point, we have available several sets of experiments with which we can measure the values of the material parameters τ_r, κ, and η.

2.5 Polymeric jamming in uniaxial extension

The results of the previous sections show that part of the flow-type dependence of the material response, namely the shear-thinning behavior versus rate-independence in

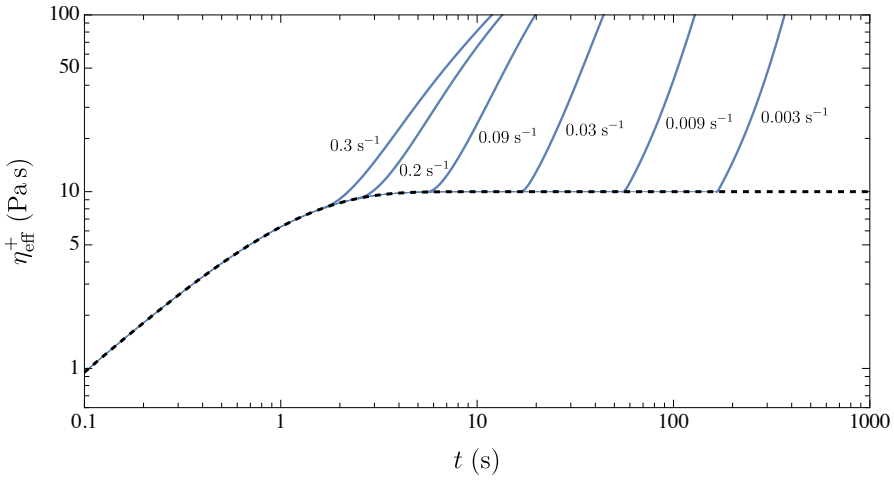

Figure 2.6: *With a strain-dependent relaxation time we can capture polymeric jamming.* The growth of the effective viscosity η^+_{eff} in uniaxial extension features a rate-independent segment (black dashed line) followed until the rate-dependent time $\gamma_{\text{J}}/\dot{\gamma}$, after which we observe a fast increase (solid lines) due to the rapidly growing relaxation time. Values of $\dot{\gamma}$ label the different data curves. The values of model parameters for this example are $\tau_{\text{r}}^0 = 1$ s, $\gamma_{\text{J}} = 0.5$, $\alpha = 4$, $\kappa = 10$ Pa, and $\eta = 10^{-3}$ Pa s.

extensional flows, is not related to microscopic phenomena but rather to the rotation of the principal strains in simple shear (which in this context is non that simple, after all). Nevertheless, there are further differences, such as extensional thickening or the impossibility of reaching a steady state, that cannot be captured with the simplest constant-parameter model.

Here we propose a mechanism and a model that can explain some features of extensional rheology, focusing on uniaxial extension for definiteness. We argue that the typical experimental realization of uniaxial extension can lead, for some fluids, to the phenomenon of polymeric jamming. That is, molecular chains that are mostly elongated in one direction and, due to the confinement in filament stretching experiments, compressed in the orthogonal plane become progressively unable to relax. We do not expect a similar phenomenon in simple shear flows where confinement does not change over time. Note that this type of effect is not necessarily related to the bulk rheology of the material, but rather to its interaction with the experimental setup, meaning that it may not appear in large-scale extensional flows.

A very rough model for polymeric jamming can be set up by letting the relaxation time τ_{r} depend on a measure of the total strain such as $\gamma(t) = \dot{\gamma}t$, which is obviously related to the filament shrinking. In particular, we fix a threshold $\gamma_{\text{J}} > 0$ and we assume that $\tau_{\text{r}} = \tau_{\text{r}}^0$, with τ_{r}^0 constant and finite, as long as $\gamma(t) < \gamma_{\text{J}}$, whereas $\tau_{\text{r}} = \tau_{\text{r}}^0 e^{\alpha(\gamma(t)-\gamma_{\text{J}})}$ if $\gamma(t) \geq \gamma_{\text{J}}$. Note that the energy balance (2.12) still applies to this model. The exponential growth of τ_{r} is, at this stage, an arbitrary modelling choice to have the material approach a solid one ($\tau_{\text{r}} = +\infty$) rather fast. It is possible to solve equation (2.20) analytically in

the region with growing τ_r, but the expression of the solution is not quite informative, and numerical integration is equally effective. The parameter $\alpha > 0$ determines the slope of the effective viscosity η^+_eff beyond the jamming strain. Indeed, with this model we predict a rate-independent behavior in the initial (rate-dependent) interval $[0, \gamma_\mathrm{J}/\dot\gamma]$, with $\eta^+_\mathrm{eff}(t) = \kappa\tau^0_\mathrm{r}(1 - e^{-t/\tau^0_\mathrm{r}}) + \eta$, followed by a fast increase, with a slope that looks approximately the same in log-scale for $\dot\gamma$ sufficiently small, and no steady state is attained. By choosing $\alpha = 4$, we obtain a picture, in Figure 2.6, that is in striking qualitative agreement with Series PSII in Figure 3.5-2 of [13], reprinted in the Appendix. This provides a strong indication that our model can capture the mechanism behind the experimental observation.

2.6 Developing models from experimental data

As shown above, to reproduce experimental results we generally need to go beyond the constant-parameter model. Especially if we wish to achieve a quantitative description of real fluids, we cannot ignore the presence of multiple relaxation mechanisms. From the microscopic perspective, we can argue that an increase of the average kinetic energy of the polymeric molecules can activate different relaxation pathways. Neglecting temperature effects, we can include this fact in our macroscopic description by letting the effective relaxation time τ_r depend on the local strain rate. This is in keeping with classical approaches, as pioneered by White and Metzner [55].

Regarding material functions in the steady-state regime, we can start from the equation solved by B_el, namely

$$\log \mathsf{B}_\mathrm{el} = \mathsf{B}_\mathrm{el}^{-1}(\tau_\mathrm{r}\nabla\boldsymbol{u})\mathsf{B}_\mathrm{el} + (\tau_\mathrm{r}\nabla\boldsymbol{u})^\mathsf{T}, \tag{2.25}$$

to see that the dependence of the elastic stress on the shear rate $\dot\gamma$ is only through the dimensionless Weissenberg number $Wi = \dot\gamma\tau_\mathrm{r}$, even when τ_r depends on $\dot\gamma$. From the practical point of view, this allows us to reconstruct the rheological curves for different models of τ_r from those obtained with constant unit values of τ_r and κ.

In small-amplitude oscillatory flows, from the solution given in Section 2.2, we see that the storage and loss moduli, G' and G'', depend on the frequency ω through the dimensionless Deborah number $De = \omega\tau_\mathrm{r}$ as long as τ_r is independent of time. Again, we can exploit this fact and consider models in which τ_r depends on ω. The rationale for this is that the maximum strain rate is proportional to ω and so the average kinetic energy available to activate relaxation pathways depends on the angular frequency as well. With this in mind, we can discuss further comparisons with experimental data.

We consider measurements of rheological properties of a wormlike micellar solution (WLM) reported by Haward & McKinley [56] and recently employed by Varchanis *et al.* [57] to evaluate the performance of various constitutive models. Regarding the linear viscoelastic properties, constant-parameter models can only capture the data in a partial way and we recover the same results of the Giesekus model, on which also the more sophisticated Vasquez–Cook–McKinley model [58] collapses (see Figure 2.7, blue dashed line). If, following the discussion above, we let the relaxation time τ_r depend on the

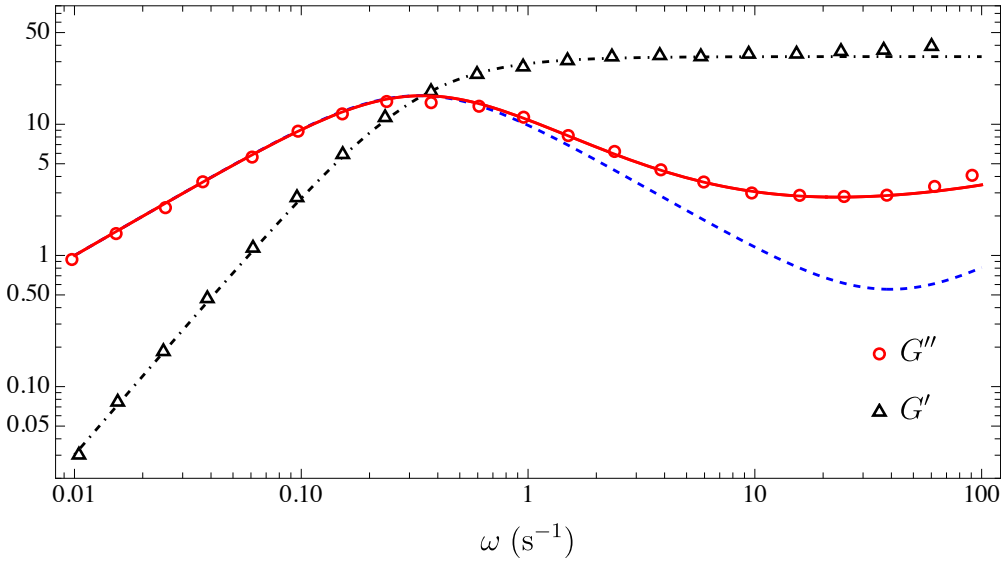

Figure 2.7: *The dependence on the angular frequency ω of the linear viscoelastic moduli G' and G'' for a WLM solution [56] can be well reproduced with an ω-dependent relaxation time.* The solid red line shows the G'' curve obtained by assuming relation (2.26) with $\tau_r^0 = 3$ s, $\alpha = 0.165$ s, and $n = 1.14$, and setting $\kappa = 33$ Pa and $\eta = 0.007$ Pa s. The result with a constant $\tau_r = 3$ s is clearly worse and it is the same that one would obtain with several other models [57]. The effect on the storage modulus G' of the varying τ_r is, in this case, hardly noticeable (dot-dashed line).

frequency according to the phenomenological law

$$\tau_r(\omega) = \frac{\tau_r^0}{1 + (\alpha\omega)^n} \tag{2.26}$$

with appropriate choices of the parameters τ_r^0, α, and n, we achieve a much better agreement with experimental data (Figure 2.7, red solid line).

Of course, many classical models are in principle amenable of such a generalisation, nevertheless it is significant to check whether the rate dependence postulated from SAOS data can be successfully applied to steady shear flows as well. To this end, we exploit the important property that, in our framework, $\log \mathsf{B}_{el}$ depends only on Wi in simple shear flows and use the data presented in Figure 2.5 to obtain a numerical interpolation of the dependence of η_{eff}/κ and Ψ_{eff}/κ on Wi. With these master curves we can retrieve the rheological predictions for any value of the parameters κ, η, and τ_r, even when τ_r depends on $\dot\gamma$. The curve that we obtain by assuming relation (2.26), with parameters fitted on the SAOS data and $\dot\gamma$ in place of ω, is already much closer to the experimental behaviour than what we obtain with constant parameters (Figure 2.8). Comparing the same model with extensional flow data (inset of Figure 2.8) we see that it captures the mild thinning behaviour, but the viscosity values are still about 30% off.

It is possible to indicate a general strategy to test whether an ω-dependent τ_r is

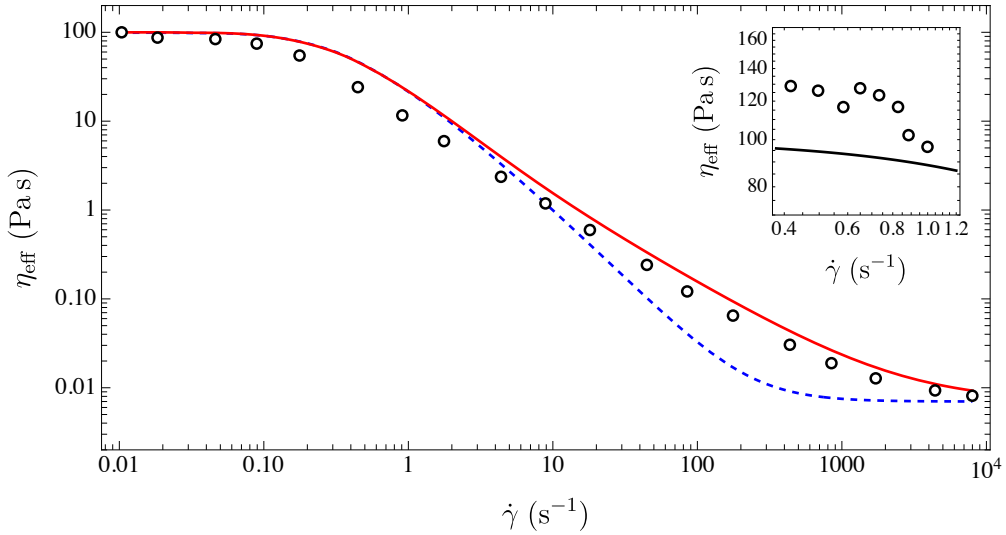

Figure 2.8: *With a rate-dependent relaxation time extrapolated from SAOS experiments we obtain an improved prediction of the steady shear viscosity.* We substitute ω with $\dot\gamma$ in the expression for $\tau_{\rm r}$ used in Figure 2.7, with identical parameters, and find the red solid curve as opposed to the blue dashed one, given by our model with constant $\tau_{\rm r}$. In the inset, we show the prediction with the same rate-dependent $\tau_{\rm r}$ of the effective viscosity in extensional flows (black solid line), that captures the trend of the experimental data (circles) in the available window of deformation rates. The experimental data are by Haward & McKinley [56] and were rescaled in the case of planar extension to match our choice of rate and viscosity.

sufficient to reproduce the measured viscoelastic moduli. If the relations (2.17)–(2.18) can describe a given material, one can deduce that

$$\tau_{\rm r}(\omega) = \frac{G'(\omega)}{\omega G''(\omega) - \omega^2 \eta}. \tag{2.27}$$

We can then extract this functional form of the relaxation time from the data and then try and see if, with such $\tau_{\rm r}(\omega)$, we can fit the experimental values of G' and G''. If the fitting is not satisfactory, we must conclude that (2.17) and (2.18) are not enough to represent the linear viscoelastic spectrum. For instance, we expect difficulties in reproducing data for materials that feature a broad spectrum of relaxation times and non-constant elastic parameter κ, such as low density polyethylene melts [59], which are usually fitted with multi-modal equations [60].

2.7 A note on dimensionless numbers

In our presentation we preferred to make use of dimensional parameters for an easier link with measurable quantities. Nevertheless, it is important to identify dimensionless parameters that can help understanding the scaling behavior of our model. The most

common dimensionless numbers related to viscoelastic fluids are the Deborah (De) and Weissenberg (Wi) numbers (see the note by Dealy [61] for a clear discussion of their definition). Clearly, they both compare the relaxation time τ_r with a characteristic rate associated with the fluid flow and remain relevant also in our model. In fact, $De = 1$ and $Wi = 1$ mark important transition points in the frequency- and rate-dependence of the material functions, respectively. This can be seen from Figures 2.2 and 2.5, where the choice $\tau_\mathrm{r} = 1$ s allows to view the plots as if the appropriate dimensionless numbers were on the horizontal axis.

Our model, in comparison with that of a Newtonian fluid, features two extra parameters, τ_r and κ. Given that the former leads to De or Wi, depending on the flow, we clearly need to introduce another dimensionless group. To quantify the overall relative importance between the plastic dissipation due to elasticity and viscous forces (with no reference to a specific flow) we can consider the quantity $(\kappa\tau_\mathrm{r} + \eta)/\eta$. This number is very useful in two ways: first, it describes the (log-scale) range within which the effective viscosity can vary; second, it represents the relative importance of plasticity with respect to viscosity in the material response observed at low values of De in oscillatory flows. At high values of $De = \omega\tau_\mathrm{r}$, the dissipation is mostly viscous, plasticity does not intervene, and the material response is that of a viscoelastic solid.

The situation in flows with constant strain rate is more involved. First of all, we should stress that using the ratio of the first normal stress difference over the shear stress to measure the degree of elasticity or nonlinearity of the fluid is misleading. In fact, such a ratio becomes $\dot\gamma\Psi_\mathrm{eff}/\eta_\mathrm{eff}$, a quantity that is identically zero in extensional flows, irrespective of the presence of elastic stresses. We then consider the definition $Wi = \dot\gamma\tau_\mathrm{r}$ (independent of the flow type) and observe that, in extensional flows, Wi is hardly relevant, since the stress growth and steady state are rate-independent. In simple shear, we can conclude that for large Wi the behavior of the fluid is essentially viscous. This is due to the fact that a faster rotation of the principal directions of the elastic stress makes relaxation more efficient, leading to smaller values of the elastic strain and, consequently, stress.

Chapter 3

Numerical simulation

The Finite Element Method (FEM) is a numerical technique used to approximate solutions to a wide range of engineering and physical problems governed by partial differential equations (PDEs) [31, 62]. It is a flexible approach that has become a cornerstone in the fields of computational engineering and applied mathematics. It is widely used in engineering for the analysis of structures, heat transfer, fluid flow, and other physical phenomena.

The primary goal of the finite element method is to break down a complex physical domain into simpler and more manageable subdomains, the finite elements. These elements are interconnected at specific nodes, forming a discretised representation of the original system. By doing so, the continuous problem defined by a PDE is transformed into a system of algebraic equations, which are then solved numerically.

3.1 Weak formulation and time discretisation

To apply the FEM discretization, we need to express the differential problem in the weak or variational formulation, that is a form suitable for the analysis in a Hilbert space framework. Indeed, the FEM approach is based on projections on subspaces with orthonormal basis functions.

We shall now present the weak formulation of (2.3)–(2.6) with the divergence-free constraint and without external forces. Formally, we multiply the differential equations by test functions $\boldsymbol{v}$, q and the tensor Φ for each $t > 0$, then integrate on Ω, where Ω is the spatial domain in $\mathbb{R}^d$. We denote by Γ_0 the portion of the boundary on which Dirichlet conditions are imposed for the velocity field and set V as the Sobolev space of divergence-free vector fields that vanish on Γ_0 and have square-integrable gradients.

By introducing the finite-difference discretisation of the time derivatives

$$\frac{\partial \boldsymbol{u}}{\partial t} = \frac{\boldsymbol{u} - \boldsymbol{u}_n}{\Delta t} \qquad \text{and} \qquad \frac{\partial \mathsf{B}_{\mathrm{el}}}{\partial t} = \frac{\mathsf{B}_{\mathrm{el}} - \mathsf{B}_{\mathrm{el,n}}}{\Delta t}, \tag{3.1}$$

where the subscript n denotes a quantity at the previous time step, we can obtain the time-discrete variational formulation as the problem of finding $\boldsymbol{u} \in V$ and square-integrable p

and $\log \mathsf{B}_{\mathrm{el}}$ such that

$$a_1\big((\boldsymbol{u},p),(\boldsymbol{v},q)\big) = L_1(\boldsymbol{v},q), \tag{3.2}$$

$$a_2\big(\mathsf{B}_{\mathrm{el}},\Phi\big) = L_2(\Phi). \tag{3.3}$$

The bilinear forms a_1, a_2 and the linear forms L_1, L_2 are defined by

$$a_1\big((\boldsymbol{u},p),(\boldsymbol{v},q)\big) = \int_\Omega \left(\rho\frac{\boldsymbol{u}}{\Delta t}\cdot\boldsymbol{v} + \eta\nabla\boldsymbol{u} : \nabla\boldsymbol{v} - p\,\mathrm{div}\,\boldsymbol{v} + q\,\mathrm{div}\,\boldsymbol{u}\right)d\boldsymbol{x}, \tag{3.4}$$

$$L_1(\boldsymbol{v},q) = \int_\Omega \left(\rho\frac{\boldsymbol{u}_n}{\Delta t}\cdot\boldsymbol{v} - \rho[(\boldsymbol{u}_n\cdot\nabla)\boldsymbol{u}_n]\cdot\boldsymbol{v}\right)d\boldsymbol{x}, \tag{3.5}$$

$$\begin{aligned} a_2\big(\mathsf{B}_{\mathrm{el}},\Phi\big) = \int_\Omega \Bigg(&\frac{\mathsf{B}_{\mathrm{el}}}{\Delta t} : \Phi + [(\boldsymbol{u}_n\cdot\nabla)\mathsf{B}_{\mathrm{el}}] : \Phi \\ &- [\nabla\boldsymbol{u}_n\mathsf{B}_{\mathrm{el}} + \mathsf{B}_{\mathrm{el}}(\nabla\boldsymbol{u}_n)^{\mathsf{T}}] : \Phi + \frac{1}{\tau_{\mathrm{r}}}[\mathsf{B}_{\mathrm{el}}\log\mathsf{B}_{\mathrm{el,n}}] : \Phi\Bigg)d\boldsymbol{x}, \end{aligned} \tag{3.6}$$

$$L_2(\Phi) = \int_\Omega \frac{\mathsf{B}_{\mathrm{el,n}}}{\Delta t} : \Phi\, d\boldsymbol{x}. \tag{3.7}$$

At each time step we solve equations (3.2) and (3.3) using the FEM discretisation in the spatial domain. We employ Lagrangian elements of order 2 for the velocity $\boldsymbol{u}$, of order 1 for B_{el}, and order 0 for the pressure p. This choice is a reasonable starting point as it provides a stable method for the linear Stokes problem. The explicit treatment of the nonlinear terms and of the coupling between the two equations poses restrictions on the size of the time step. Nevertheless, it is appropriate at least for flows with moderate Reynolds and Weissenberg numbers. Steady-state solutions are obtained within this scheme as long-time limits of the evolution.

3.2 Numerical results

3.2.1 Dependence on parameters

Here we wish to illustrate how the behaviour of the constant-parameter model is affected by changing parameters in a paradigmatic flow geometry. We consider the pressure-driven flow past a cylinder of radius 0.125 m in a two-dimensional domain of length 2 m and width 1 m, which is periodic along the flow direction. With this choice of geometry, the obstacle covers one fourth of the channel cross section.

The geometry of the domain is illustrated in Figure 3.1 where we also show three different meshes with increasing refinement (the refinement parameter is the number of nodes on the vertical side of the domain). The mesh convergence of our solutions is shown by the steady-state velocity components in Figure 3.2 and 3.3 and by the non-affine pressure contribution (that is the difference between the real pressure and a fixed linear profile used to impose the total pressure gradient across the channel) in Figure 3.4. The effect of the mesh refinement on the velocity components is also shown in Figure 3.5 using five different cross-sections of the channel.

By analysing the horizontal, u_x, and vertical, u_y, velocity on the same cross-sections we observe the following. The flow rate increases with the imposed pressure gradient Γ, but we notice some numerical instability when the flow is stronger (Figure 3.6). A larger relaxation time hinders the flow, since elastic effects are more pronounced (Figure 3.7) and the same happens with larger elastic constant (Figure 3.8).

3.2.2 Simulation of WLM fluid

In this section, we present the results of simulations in which the material parameters are chosen in accordance to the values reported about wormlike micellar solutions (WLM) by Varchanis *et al.* [57].

In Figure 3.9 and 3.10 we present the flow past a cylinder obtained with an imposed flow at the left inlet that fixes the flow rate. The aim is to represent the flow in a microfluidic device where the width of the channel is 0.4 mm and the diameter of the cylinder equals 20 μm. For our simulation we use dimensionless parameters as follows. All lengths are divided by the radius R and velocities are divided by a reference U set by the imposed flow rate. The effective viscosity is $\eta_{\text{eff}} = \frac{\eta}{\rho U R}$, effective elastic constant is $\kappa_{\text{eff}} = \frac{\kappa}{\rho U^2}$, and the effective relaxation time is $\tau_{\text{eff}} = \frac{\tau_r U}{R}$.

We were able to achieve a seemingly steady state for the velocity field (lasting for a large number of integration steps) but the elastic stress is still growing. We need to ascertain whether this is due to a numerical issue or to the fact that we found a meta-stable state, but we have not reached the fully developed flow. This might explain why the velocity profile (Figure 3.10) is still quite similar to that of a Newtonian fluid, whereas we would expect a more pronounced shear-thinning behaviour.

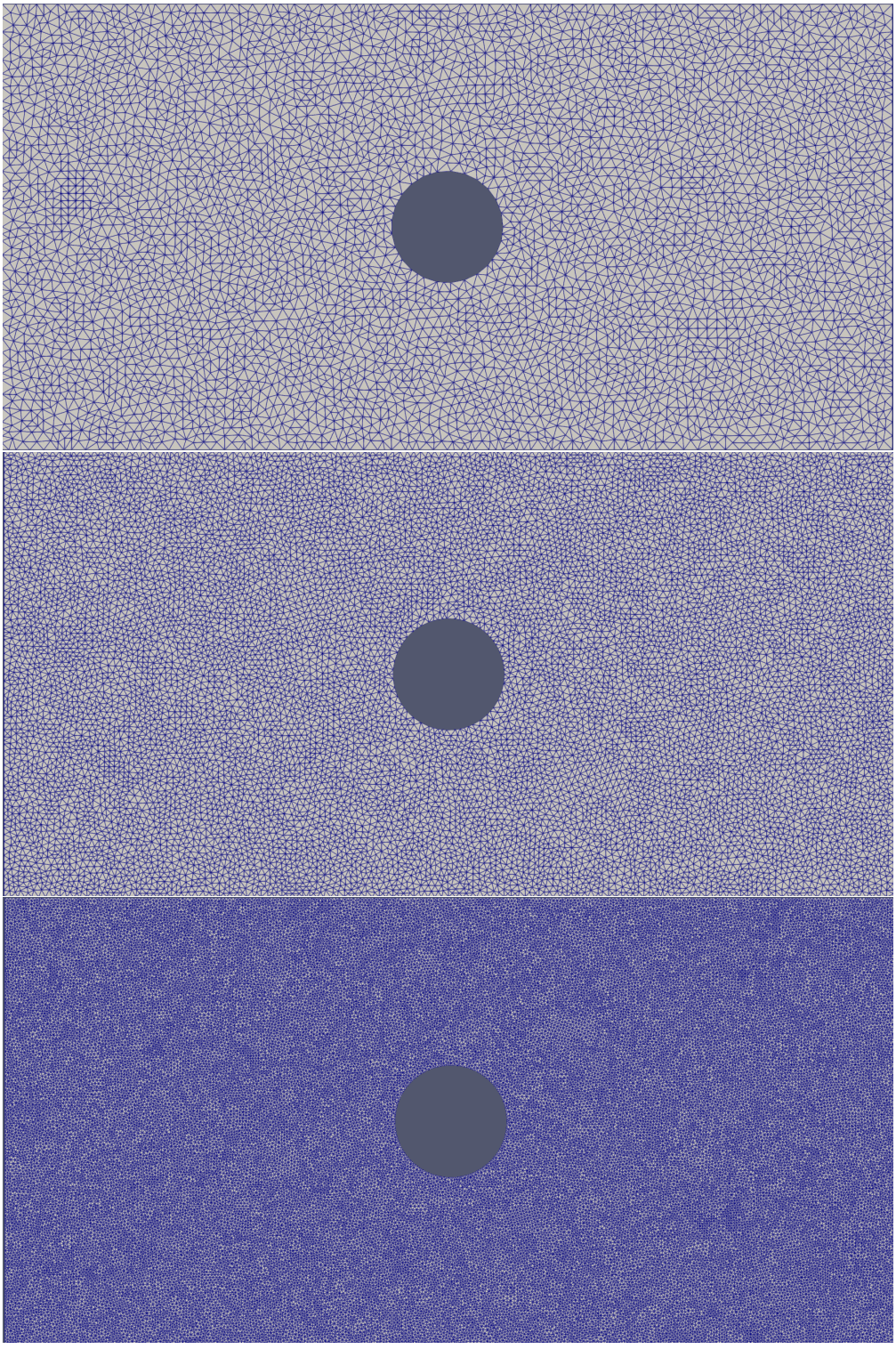

Figure 3.1: The finite-element mesh on the domain corresponding to Refinement 64, 100, and 200 from top to bottom, respectively.

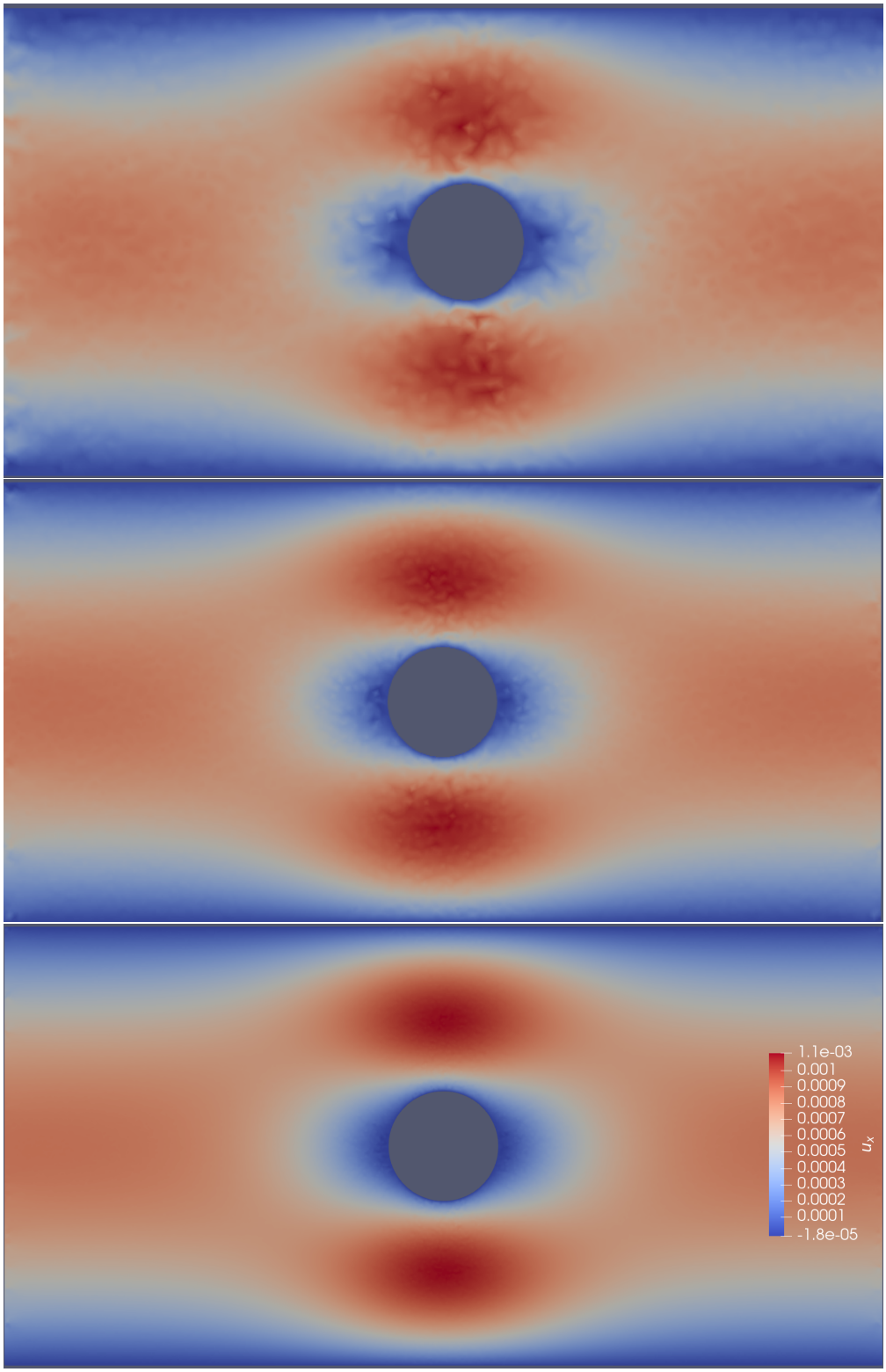

Figure 3.2: Horizontal velocity field u_x obtained by setting $T = 20$ s, $\kappa = 10$ Pa, $\eta = 1$ Pa s, $\Gamma = -2$ Pa/m, $\tau_r = 10$ s, $\Delta t = 0.01$ s and by changing Refinement 64, 100, and 200 from top to bottom respectively.

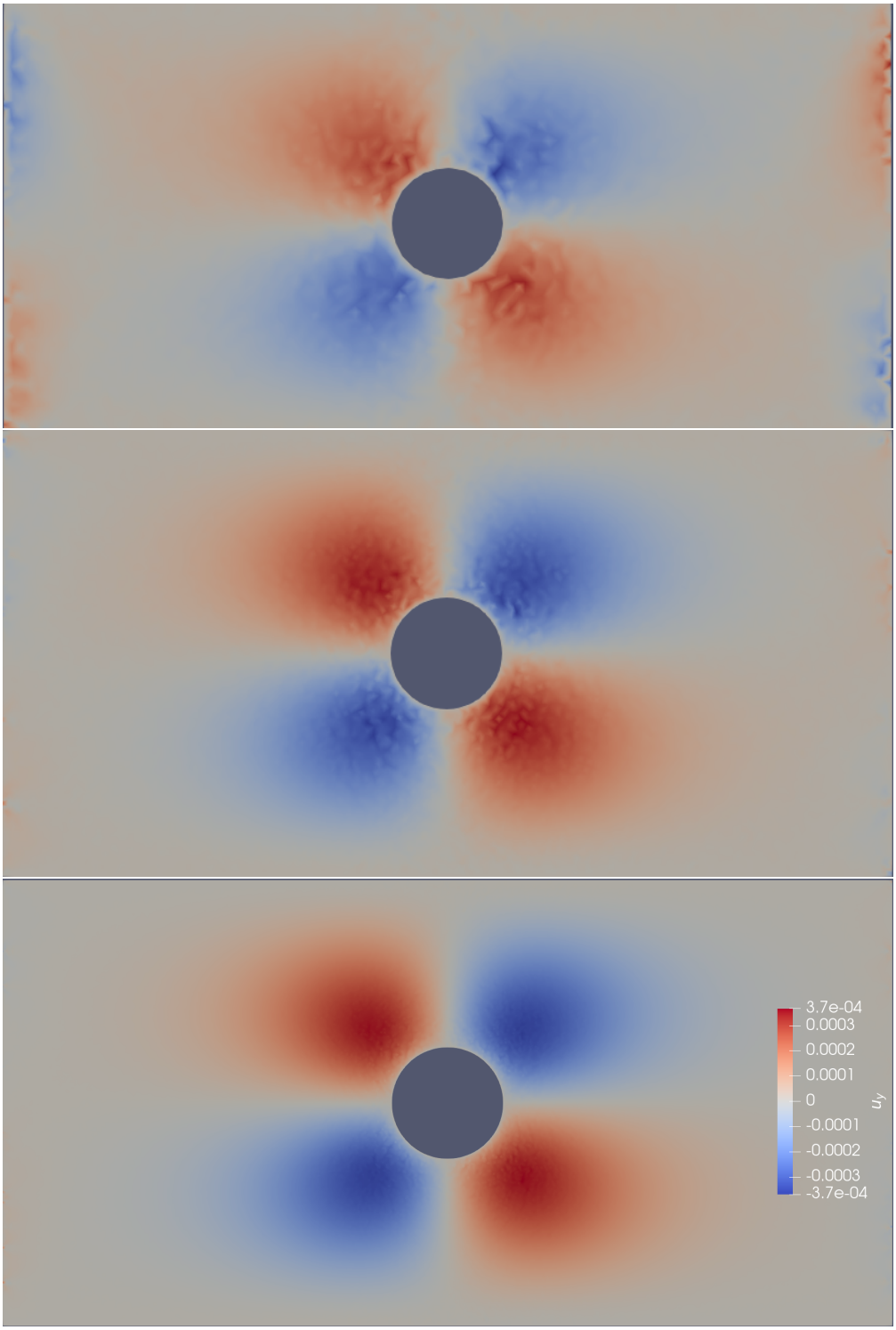

Figure 3.3: Vertical velocity field u_y obtained by setting $T = 20$ s, $\kappa = 10$ Pa, $\eta = 1$ Pa s, $\Gamma = -2$ Pa/m, $\tau_r = 10$ s, $\Delta t = 0.01$ s and by changing Refinement 64, 100, and 200 from top to bottom respectively.

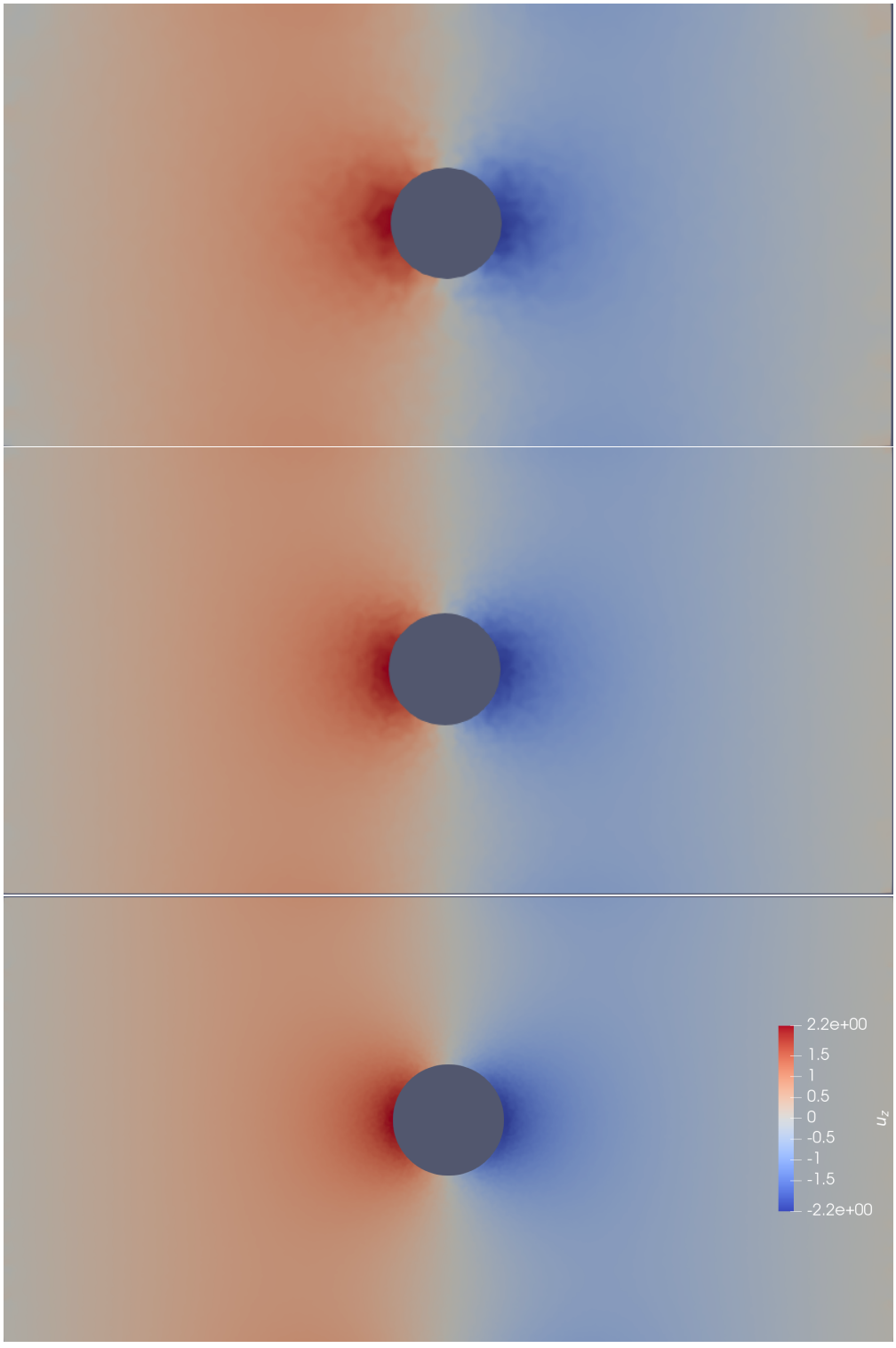

Figure 3.4: The non affine pressure p obtained by setting $T = 20$ s, $\kappa = 10$ Pa, $\eta = 1$ Pa s, $\Gamma = -2$ Pa/m, $\tau_r = 10$ s, $\Delta t = 0.01$ s and by changing Refinement 64, 100, and 200 from top to bottom respectively.

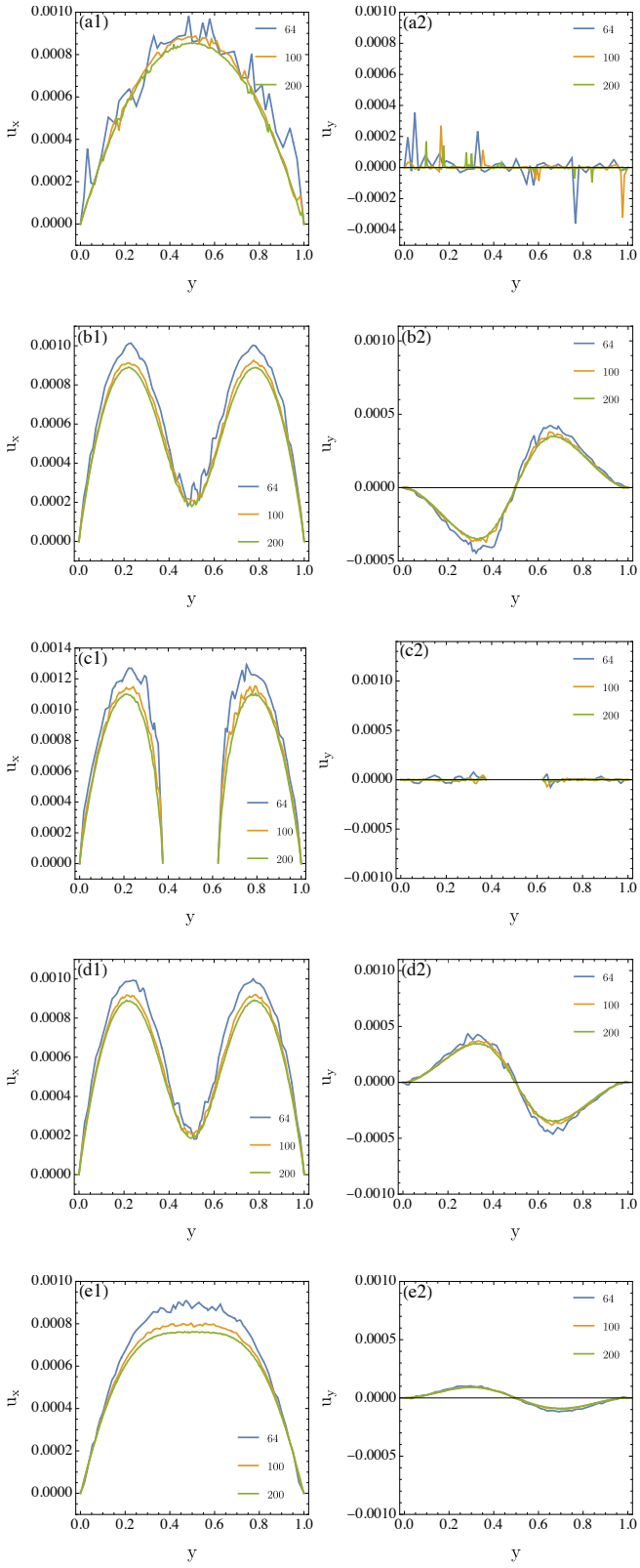

Figure 3.5: Velocity field $\boldsymbol{u}$ obtained by setting $T = 20$ s, $\tau_r = 10$ s, $\kappa = 10$ Pa, $\Gamma = -1$ Pa/m, $\eta = 1$ Pa s, $\Delta t = 0.01$ s and by changing Refinement as indicated by the curve labels. The sections of the domain are: (a) $\{x = 0\}$, (b) $\{x = 0.8\}$, (c) $\{x = 1\}$, (d) $\{x = 1.2\}$, (e) $\{x = 1.5\}$. We observe that, by increasing the mesh refinement, both the horizontal and vertical velocity components u_x and u_y are more precise and converge.

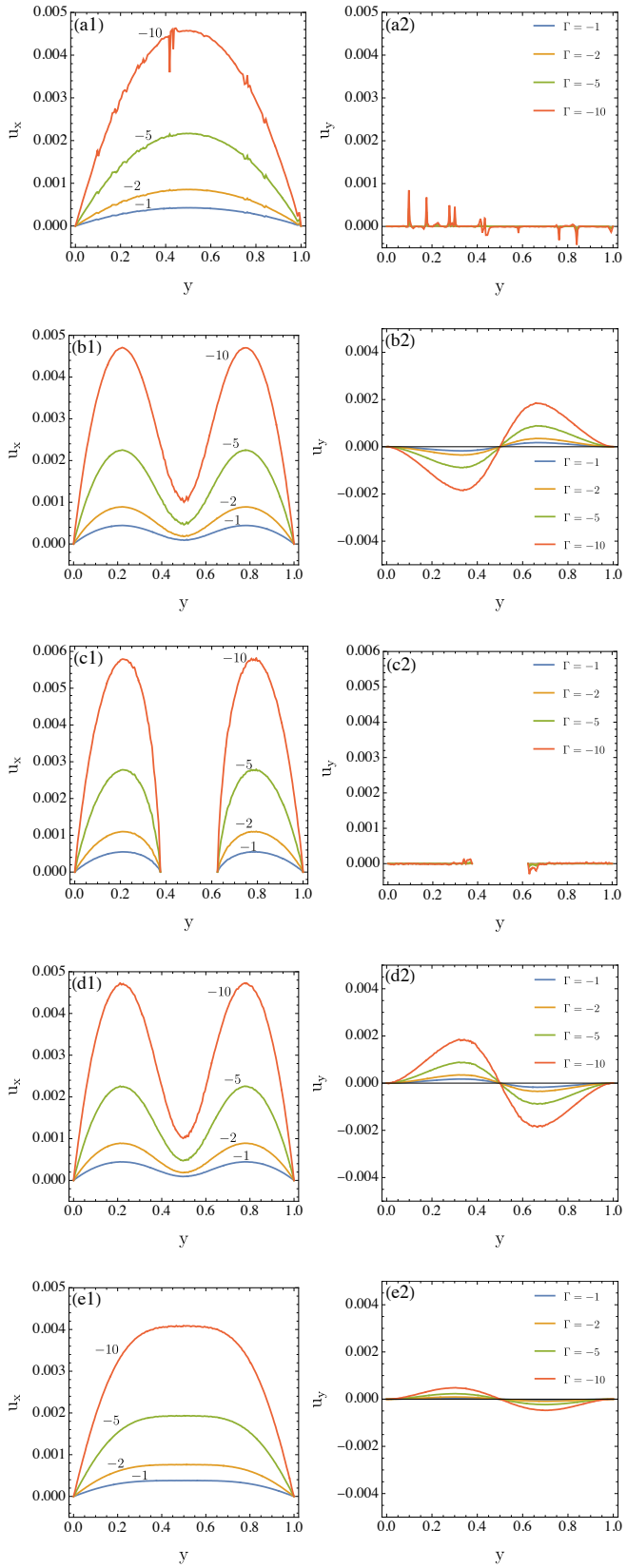

Figure 3.6: Velocity field $\boldsymbol{u}$ obtained by setting $T = 20$ s, $\kappa = 10$ Pa, $\eta = 1$ Pa s, $\tau_r = 10$ s, $\Delta t = 0.01$ s and by changing Γ as indicated by the curve labels. The sections of the domain are: (a) $\{x = 0\}$, (b) $\{x = 0.8\}$, (c) $\{x = 1\}$, (d) $\{x = 1.2\}$, (e) $\{x = 1.5\}$. From this graphs, we notice that when the absolute value of the pressure drop Γ is increased, the intensity of the velocity field increases in a linear fashion. Notice that our simulations are all in a non-turbulent regime.

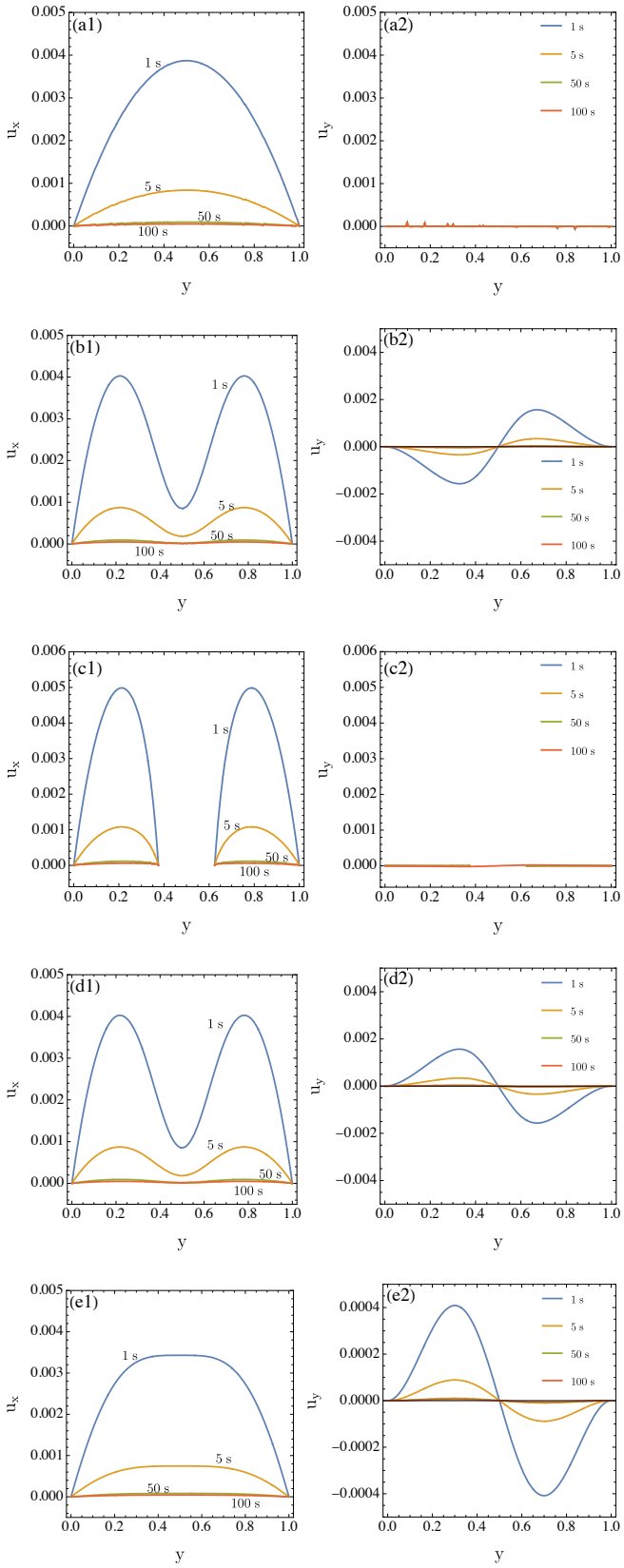

Figure 3.7: Velocity field $\boldsymbol{u}$ obtained by setting $T = 20$ s, $\kappa = 10$ Pa, $\Gamma = -1$ Pa/m, $\eta = 1$ Pa s, $\Delta t = 0.01$ s and by changing τ_r as indicated by the curve labels. The sections of the domain are: (a) $\{x = 0\}$, (b) $\{x = 0.8\}$, (c) $\{x = 1\}$, (d) $\{x = 1.2\}$, (e) $\{x = 1.5\}$. We observe that by increasing the relaxation time τ_r the elastic response becomes more important and the flow is progressively hindered.

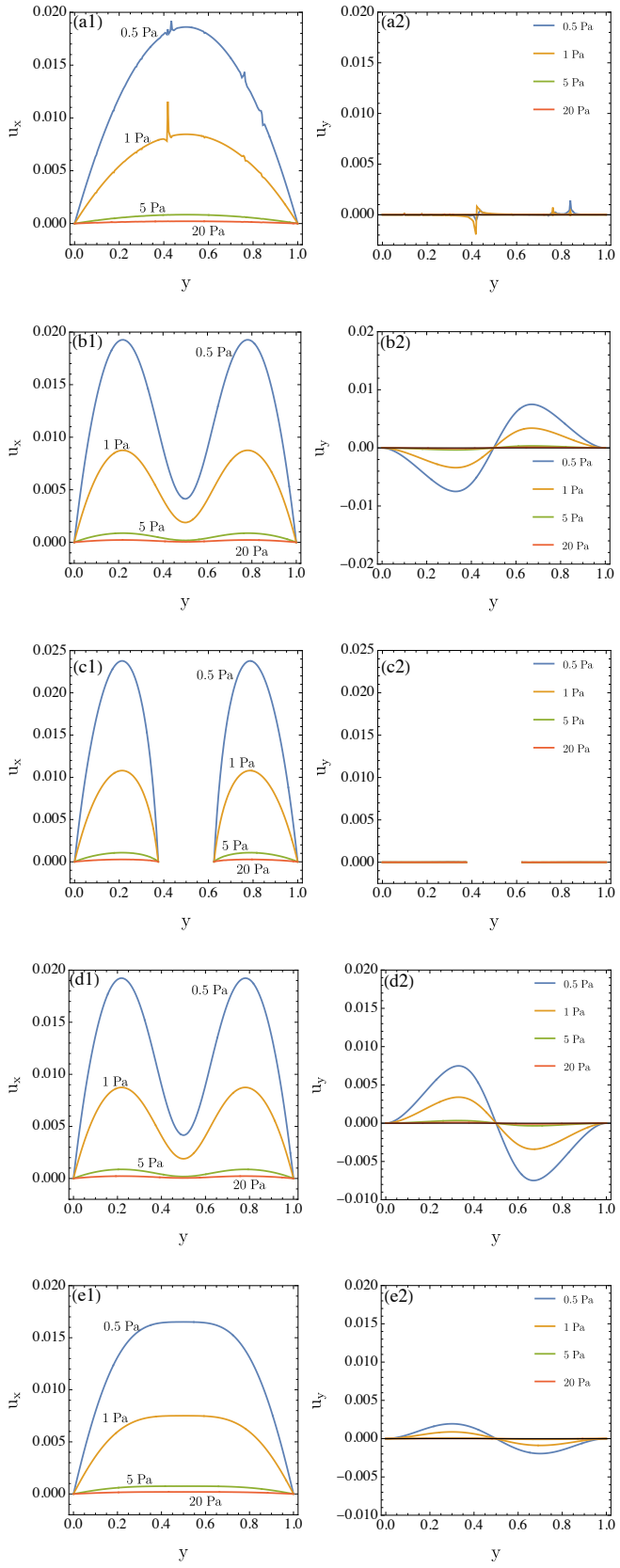

Figure 3.8: Velocity field $\boldsymbol{u}$ obtained by setting $T = 20$ s, $\tau_r = 10$ s, $\Gamma = -1$ Pa/m, $\eta = 1$ Pa s, $\Delta t = 0.01$ s and by changing κ as indicated by the curve labels. The sections of the domain are: (a) $\{x = 0\}$, (b) $\{x = 0.8\}$, (c) $\{x = 1\}$, (d) $\{x = 1.2\}$, (e) $\{x = 1.5\}$. Also increasing the elastic modulus κ we obtain more resistance to flowing and the velocity becomes smaller and smaller.

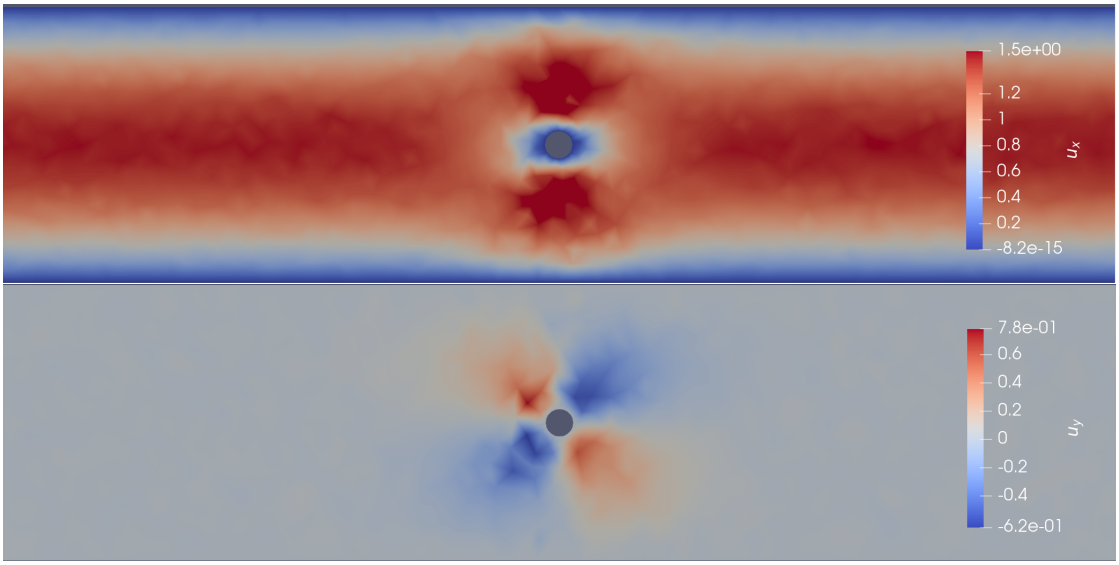

Figure 3.9: Horizontal (top) and vertical (bottom) velocity field obtained by setting the dimensionless time $TU/R = 0.004$, $\kappa = 28.5$ Pa, $\eta = 0.005$ Pa s, $\tau_r = 1.8$ s, $U\Delta/Rt = 2 \times 10^{-7}$ and Refinement 100. The velocity field reached a seemingly steady state albeit with some evident numerical noise, possibly due to the inhomogeneity of the elastic stress.

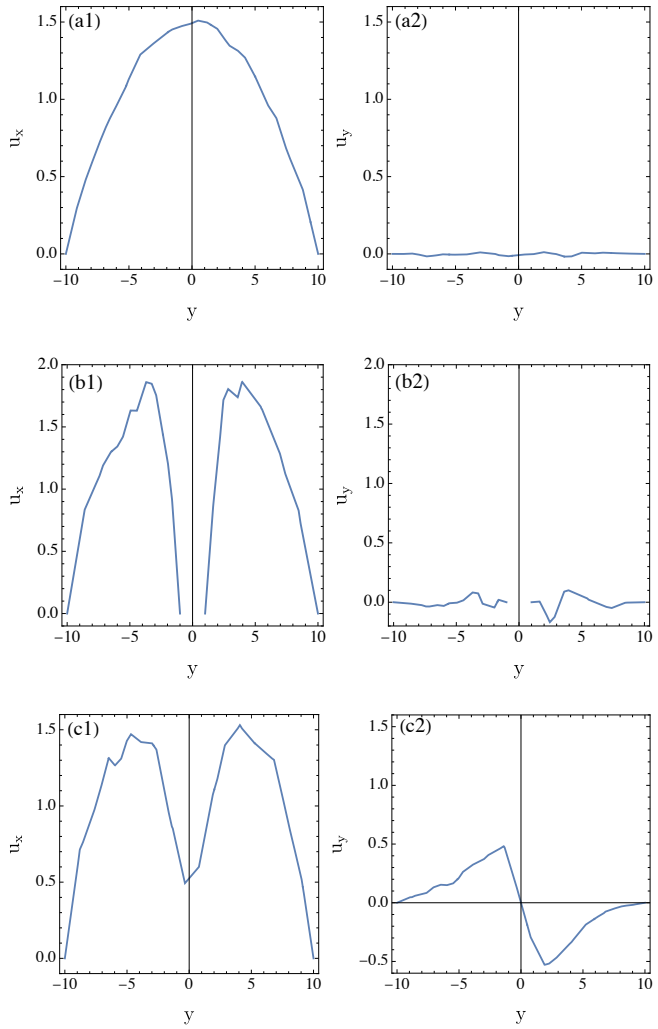

Figure 3.10: Velocity field $\boldsymbol{u}$ obtained by setting $TU/R = 0.004$, $\tau_r = 1.8$ s, $\kappa = 28.5$ Pa, $\eta = 0.005$ Pa s, $U\Delta t/R = 2 \times 10^{-7}$ and Refinement 100. The sections of the domain are: (a) $\{x = -50\}$, (b) $\{x = 0\}$, (c) $\{x = 2.5\}$. The quality of the velocity profile is still to be improved. It reamins quite similar to that of a Newtonian fluid, probably due to the presence of a meta-stable state in the experimental regime that we are trying to reproduce. Further improvements of the numerical method will be implemented to obtain a better result.

Chapter 4

Conclusions

We introduced a class of tensorial models aimed at describing viscoelastic materials. The cornerstones of this framework are an elastic stress that depends logarithmically on a suitable measure of strain and the choice of letting the elastic strain evolution emerge from two distinct evolution equations, one for the current deformation and the other for a tensorial descriptor of the elastically-relaxed state. While the former is a necessary kinematic relation between velocity and deformation, the latter involves constitutive choices that are based on arguments borrowed from solid plasticity. Our line of thought differs considerably from the classical Oldroyd's approach. Even though we can derive an equation for a quantity akin to a conformation tensor, the objective rate entering its evolution is not a matter of choice, as it descends directly from the kinematic evolution of the current deformation gradient. We stress that, in our framework, viscoelastic fluids emerge as an interpolation between purely viscous fluids and solids, controlled by a relaxation time parameter ranging from zero (viscous fluid) to infinity (viscoelastic solid).

We have shown that a simple model with constant material parameters performs very well in reproducing the behavior of viscoelastic fluids observed in rheometric experiments. Moreover, it helps understanding the origin of the difference in extensional and shear rheology and the relative importance of viscous, elastic, and plastic effects. Another important feature of this model is that it avoids the erroneous prediction of an exponential growth of the elastic stress in extensional flows that sometimes arises in connection with elastic models of neo-Hookean type.

To approach the modelling of real fluids, it is important to consider the presence of multiple relaxation times. This can be done within our framework by letting the relaxation time parameter depend on other relevant quantities. We provide a first example of what can be achieved in this way by addressing a situation in which an abrupt change in the elastic response during uniaxial extension prevents the attainment of steady flows. Our findings suggest the presence of a phenomenon that can be described as a progressive polymeric jamming, in which the relaxation time diverges due to the experiment geometry. We have also shown how to capture the rheological behaviour of wormlike micellar solutions by means of a rate-dependent relaxation time. Meanwhile, we can indicate as the presence of multiple relaxation modes a challenging aspect of real fluids that may require important

generalisations of our model.

How to harness the freedom in modelling the relaxation time parameter to capture further rheological behaviors, such as viscoplastic yielding and softening, and describe different classes of complex fluids will be the subject of future research. Nevertheless, we can foresee that the phenomenon of yielding could be reproduced by setting the relaxation time equal to a sufficiently large value for small elastic strains and then letting it decrease rather dramatically once a given threshold is overcome. Different choices of such a decrease should be motivated on the basis of microscopic models to achieve a better understanding of the origin of experimental observations.

We have presented numerical solutions obtained with a finite-element discretisation of the flow problem. These results provide a basic illustration of the parameter dependence of our model. They should be considered a s a first step in the identification of an efficient simulation tool. Indeed, while we observe a satisfactory stability of our method, it is not suitable to obtain steady-state result if the transient effects require a small time step. Moreover, a better treatment of the nonlinear terms is required to explore the high-Weissenberg number regime.

Appendix: Reprinted figures

Here we present some figures, reprinted from [13] with permission, for an easier comparison with our results.

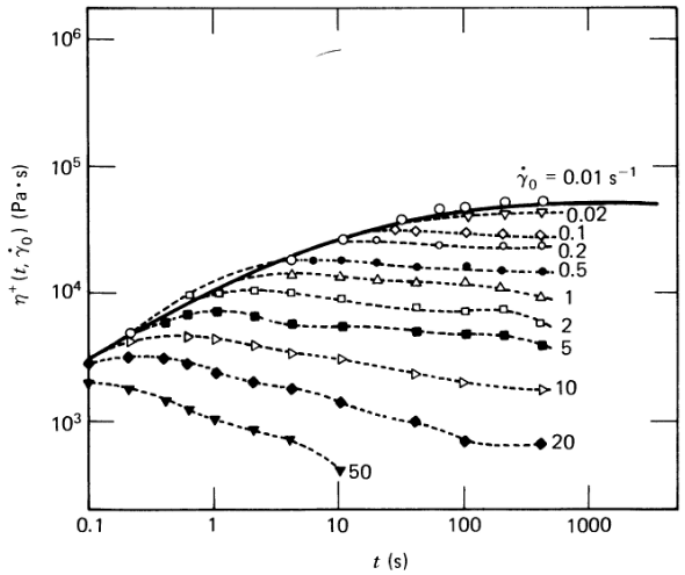

FIGURE 3.4-7. Shear stress growth function $\eta^+(t,\dot{\gamma}_0)$ data for a low-density polyethylene melt (Melt I). The maximum in η^+ occurs at smaller times as $\dot{\gamma}_0$ is increased. Note that all of the η^+ curves lie below the solid curve envelope, which is the value of η^+ in the linear viscoelastic limit. The solid curve is calculated from Eq. 5.3-25 with the spectrum in Table 5.3-2. The experimental data for small $\dot{\gamma}$ differ from the linear viscoelastic prediction at short times because of instrumental problems involved in the start-up of steady shear flow. [Reprinted with permission from M. H. Wagner and J. Meissner, *Macromol. Chem.*, **181**, 1533–1550 (1980), Hüthig and Wepf Verlag, Basel.]

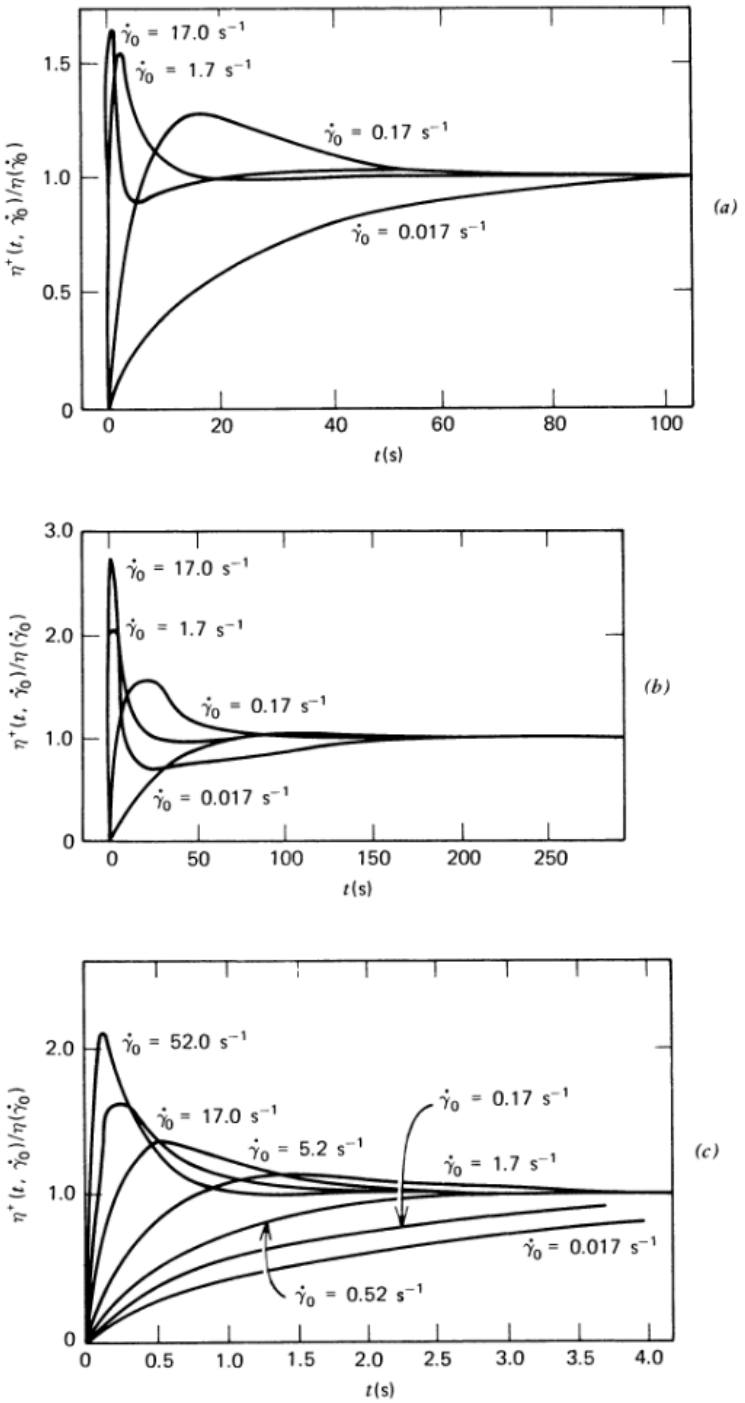

FIGURE 3.4-8. Shear stress growth function $\eta^+(t,\dot{\gamma}_0)/\eta(\dot{\gamma}_0)$ for two polymer solutions and an aluminum soap solution: (*a*) 1.5% polyacrylamide (Separan AP30) in a 50/50 mixture by weight of water and glycerin; (*b*) 2.0% polyisobutylene in Primol; and (*c*) 7% aluminum laurate in a mixture of decalin and *m*-cresol. All data were taken at 298 K. Note that the data are reduced with respect to $\eta(\dot{\gamma}_0)$ so that they all approach a common asymptote; all the data still lie within the linear viscoelastic envelope if plotted as $\eta^+(t, \dot{\gamma}_0)$. [Data of J. D. Huppler, I. F. Macdonald, E. Ashare, T. W. Spriggs, R. B. Bird, and L. A. Holmes, *Trans. Soc. Rheol.*, **11**, 181–204 (1967).]

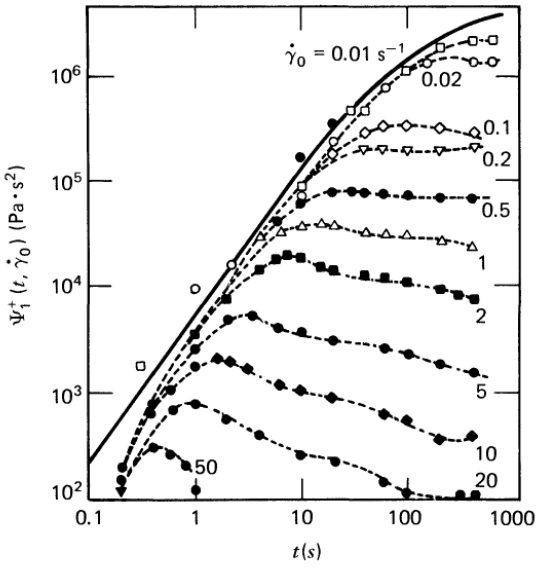

FIGURE 3.4-9. First normal stress growth function $\Psi_1^+(t, \dot{\gamma}_0)$ for the low-density polyethylene melt (Melt I) in Fig. 3.4-7. All Ψ_1^+ curves lie below the solid curve envelope which is approached for small shear rates; the solid curve is calculated from linear viscoelastic data (see Table 5.3-2) with the Lodge rubberlike liquid model (cf. Eqs. 8.2-1 and 4). [Reprinted with permission from M. H. Wagner and J. Meissner, *Macromol. Chem.*, **181**, 1533–1550 (1980), Hüthig and Wepf Verlag, Basel.]

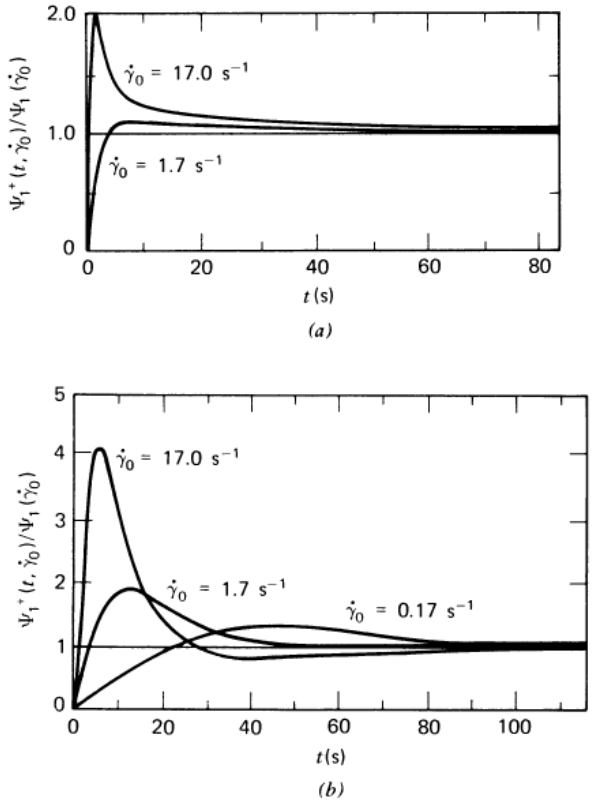

FIGURE 3.4-10. First normal stress growth function $\Psi_1^+(t, \dot{\gamma}_0)/\Psi_1(\dot{\gamma}_0)$ for (*a*) 1.5% polyacrylamide (Separan AP30) in a 50/50 mixture by weight of water and glycerin and (*b*) 2.0% polyisobutylene in Primol. All data were taken at 298 K. Note that Ψ_1^+ is reduced by the steady shear flow value Ψ_1 so that these curves show the relative sizes of the overshoot at different shear rates. [Data of J. D. Huppler, I. F. Macdonald, E. Ashare, T. W. Spriggs, R. B. Bird, and L. A. Holmes, *Trans. Soc. Rheol.*, **11**, 181–204 (1967).]

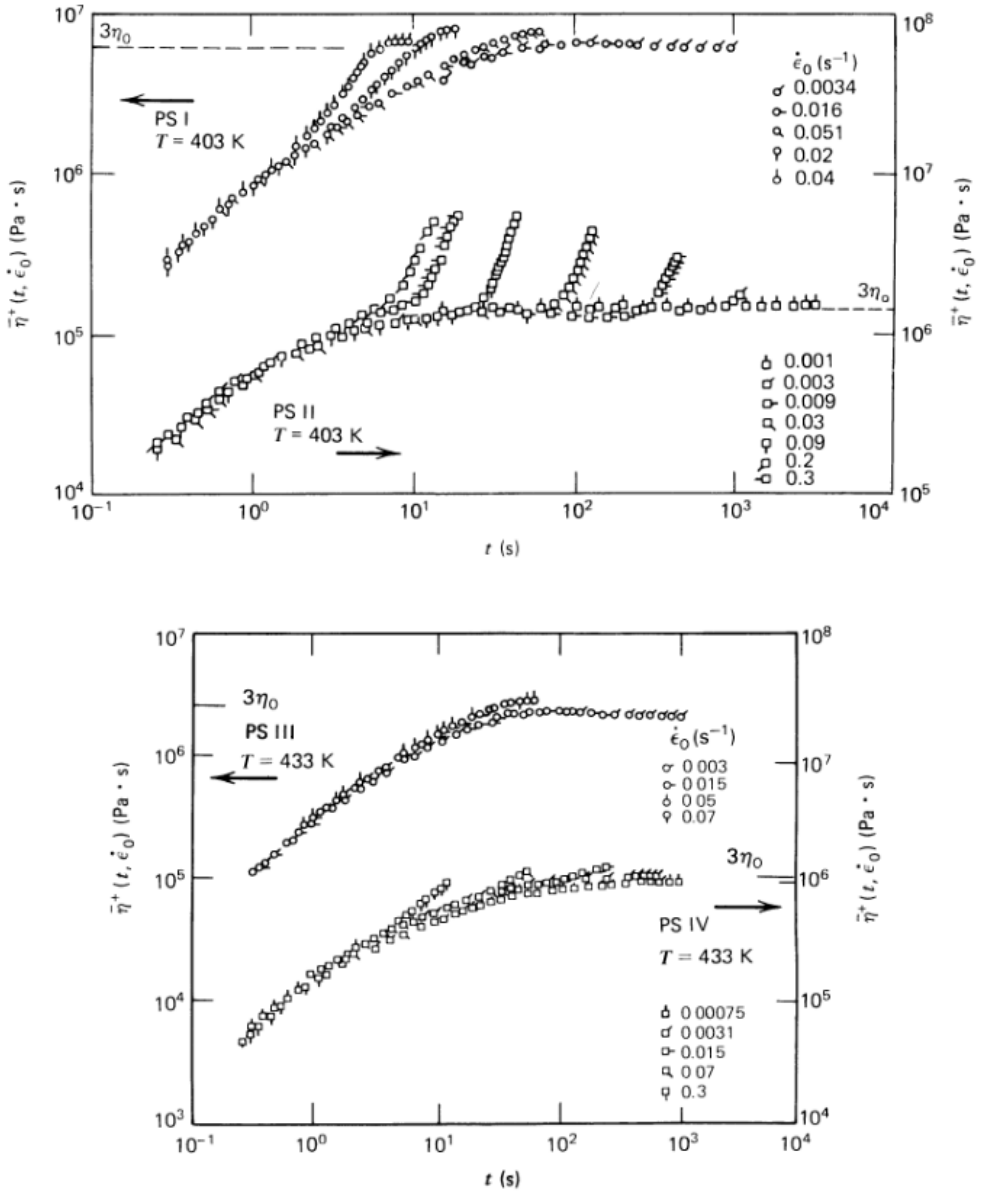

FIGURE 3.5-2. Time dependence of the elongational stress growth viscosity $\bar{\eta}^+$ for four polystyrene melts. The constant elongation rate $\dot{\varepsilon}_0$ is applied to the samples for $t \geq 0$. The number average and weight average molecular weights of the samples are as follows:

	$\bar{M}_w$	$\bar{M}_w/\bar{M}_n$
PS I	7.4×10^4	1.2
PS II	3.9×10^4	1.1
PS III	2.53×10^5	1.9
PS IV	2.19×10^5	2.3

[Data from H. Münstedt, *J. Rheol.*, **24**, 847–867 (1980).]

Bibliography

1. Oldroyd, J. G., On the formulation of rheological equations of state, *Proceedings of the Royal Society of London. Series A. Mathematical and Physical Sciences* **200,** 523–541 (1950).

2. Oldroyd, J. G., Non-Newtonian effects in steady motion of some idealized elastico-viscous liquids, *Proceedings of the Royal Society of London. Series A. Mathematical and Physical Sciences* **245,** 278–297 (1958).

3. Johnson Jr, M. & Segalman, D., A model for viscoelastic fluid behavior which allows non-affine deformation, *Journal of Non-Newtonian fluid mechanics* **2,** 255–270 (1977).

4. White, J. & Metzner, A., Development of constitutive equations for polymeric melts and solutions, *Journal of Applied Polymer Science* **7,** 1867–1889 (1963).

5. Giesekus, H., Die elastizität von flüssigkeiten, *Rheologica Acta* **5,** 29–35 (1966).

6. Bird, R. B. & Carreau, P. J., A nonlinear viscoelastic model for polymer solutions and melts—I, *Chemical Engineering Science* **23,** 427–434 (1968).

7. Marrucci, G., The free energy constitutive equation for polymer solutions from the dumbbell model, *Transactions of the Society of Rheology* **16,** 321–330 (1972).

8. Gordon, R. & Schowalter, W., Anisotropic fluid theory: a different approach to the dumbbell theory of dilute polymer solutions, *Transactions of the Society of Rheology* **16,** 79–97 (1972).

9. Acierno, D., La Mantia, F., Marrucci, G. & Titomanlio, G., A non-linear viscoelastic model with structure-dependent relaxation times: I. Basic formulation, *Journal of Non-Newtonian Fluid Mechanics* **1,** 125–146 (1976).

10. Phan-Thien, N. & Tanner, R. I., A new constitutive equation derived from network theory, *Journal of Non-Newtonian Fluid Mechanics* **2,** 353–365 (1977).

11. Phan-Thien, N., A nonlinear network viscoelastic model, *Journal of Rheology* **22,** 259–283 (1978).

12. Beris, A. N., Continuum mechanics modeling of complex fluid systems following Oldroyd's seminal 1950 work, *Journal of Non-Newtonian Fluid Mechanics* **298,** 104677 (2021).

13. Bird, R. B., Armstrong, R. C. & Hassager, O., *Dynamics of polymeric liquids. Vol. 1: Fluid mechanics* (John Wiley and Sons Inc., New York, NY, 1987).

14. Beris, A. N. & Edwards, B. J., *Thermodynamics of flowing systems: with internal microstructure* (Oxford University Press, USA, 1994).

15. Phan-Thien, N. & Mai-Duy, N., *Understanding viscoelasticity: an introduction to rheology* (Springer, 2013).

16. Salmon, J.-B., Colin, A., Manneville, S. & Molino, F., Velocity profiles in shear-banding wormlike micelles, *Physical review letters* **90,** 228303 (2003).

17. Miller, E. & Rothstein, J. P., Transient evolution of shear-banding wormlike micellar solutions, *Journal of Non-Newtonian Fluid Mechanics* **143,** 22–37 (2007).

18. Hu, Y. T. & Lips, A., Kinetics and mechanism of shear banding in an entangled micellar solution, *Journal of Rheology* **49,** 1001–1027 (2005).

19. Appell, J., Porte, G., Khatory, A., Kern, F. & Candau, S., Static and dynamic properties of a network of wormlike surfactant micelles (cetylpyridinium chlorate in sodium chlorate brine), *Journal de Physique II* **2,** 1045–1052 (1992).

20. Cates, M. & Candau, S., Statics and dynamics of worm-like surfactant micelles, *Journal of Physics: Condensed Matter* **2,** 6869 (1990).

21. Candau, S. & Oda, R., Linear viscoelasticity of salt-free wormlike micellar solutions, *Colloids and Surfaces A: Physicochemical and Engineering Aspects* **183,** 5–14 (2001).

22. Davies, T. S., Ketner, A. M. & Raghavan, S. R., Self-assembly of surfactant vesicles that transform into viscoelastic wormlike micelles upon heating, *Journal of the American Chemical Society* **128,** 6669–6675 (2006).

23. Raghavan, S. R., Distinct character of surfactant gels: a smooth progression from micelles to fibrillar networks, *Langmuir* **25,** 8382–8385 (2009).

24. Kefi, S. *et al.,* Expanding applications for viscoelastic surfactants, *Oilfield Rev* **16,** 10–23 (2004).

25. Rehage, H. & Hoffmann, H., Viscoelastic surfactant solutions: model systems for rheological research, *Molecular Physics* **74,** 933–973 (1991).

26. Turner, M. & Cates, M., Linear viscoelasticity of wormlike micelles: A comparison of micellar reaction kinetics, *Journal de Physique II* **2,** 503–519 (1992).

27. Porte, G., Berret, J.-F. & Harden, J. L., Inhomogeneous flows of complex fluids: Mechanical instability versus non-equilibrium phase transition, *Journal de Physique II* **7,** 459–472 (1997).

28. Haward, S. J. & McKinley, G. H., Stagnation point flow of wormlike micellar solutions in a microfluidic cross-slot device: Effects of surfactant concentration and ionic environment, *Physical Review E* **85,** 031502 (2012).

29. Prud'homme, R. K. & Warr, G. G., Elongational flow of solutions of rodlike micelles, *Langmuir* **10,** 3419–3426 (1994).

30. Rothstein, J. P., Transient extensional rheology of wormlike micelle solutions, *Journal of Rheology* **47,** 1227–1247 (2003).

31. Larson, M. G. & Bengzon, F., *The finite element method: theory, implementation, and applications* (Springer Science & Business Media, 2013).

32. Geankoplis, C. J., *Transport Processes and Unit Operations* (Prentice Hall, 1993).

33. Morrison, F. A., *Understanding rheology* (Oxford University Press, 2001).

34. Oldroyd, J. G., On the formulation of rheological equations of state, *Proceedings of the Royal Society of London. Series A. Mathematical and Physical Sciences* **200,** 523–541 (1950).

35. Green, M. S. & Tobolsky, A. V., A new approach to the theory of relaxing polymeric media, *The Journal of chemical physics* **14,** 80–92 (1946).

36. Kuhn, W., Über die gestalt fadenförmiger moleküle in lösungen, *Kolloid-Zeitschrift* **68,** 2–15 (1934).

37. Rouse Jr, P. E., A theory of the linear viscoelastic properties of dilute solutions of coiling polymers, *The Journal of Chemical Physics* **21,** 1272–1280 (1953).

38. Gordon, R. & Schowalter, W., Anisotropic fluid theory: a different approach to the dumbbell theory of dilute polymer solutions, *Transactions of the Society of Rheology* **16,** 79–97 (1972).

39. Giesekus, H., A simple constitutive equation for polymer fluids based on the concept of deformation-dependent tensorial mobility, *Journal of Non-Newtonian Fluid Mechanics* **11,** 69–109 (1982).

40. Snoeijer, J., Pandey, A., Herrada, M. & Eggers, J., The relationship between viscoelasticity and elasticity, *Proceedings of the Royal Society A* **476,** 20200419 (2020).

41. Xiao, H., Bruhns, O. & Meyers, A., A consistent finite elastoplasticity theory combining additive and multiplicative decomposition of the stretching and the deformation gradient, *International Journal of Plasticity* **16,** 143–177 (2000).

42. Xiao, H., Bruhns, O. & Meyers, A., Explicit dual stress-strain and strain-stress relations of incompressible isotropic hyperelastic solids via deviatoric Hencky strain and Cauchy stress, *Acta Mechanica* **168,** 21–33 (2004).

43. Neff, P., Eidel, B. & Martin, R. J., Geometry of logarithmic strain measures in solid mechanics, *Archive for Rational Mechanics and Analysis* **222,** 507–572 (2016).

44. Pruuvsa, V., Rajagopal, K. & Tuma, K., Gibbs free energy based representation formula within the context of implicit constitutive relations for elastic solids, *International Journal of Non-Linear Mechanics* **121,** 103433 (2020).

45. Gurtin, M. E., Fried, E. & Anand, L., *The mechanics and thermodynamics of continua* (Cambridge University Press, 2010).

46. Kröner, E., Allgemeine kontinuumstheorie der versetzungen und eigenspannungen, *Archive for Rational Mechanics and Analysis* **4,** 273–334 (1959).

47. Lee, E. & Liu, D., Finite-strain elastic—plastic theory with application to plane-wave analysis, *Journal of applied physics* **38,** 19–27 (1967).

48. Lee, E. H., Elastic-plastic deformation at finite strains, *Journal of Applied Mechanics* **36,** 1–6 (1969).

49. DiCarlo, A. & Quiligotti, S., Growth and balance, *Mechanics Research Communications* **29,** 449–456 (2002).

50. Taber, L. A., Towards a unified theory for morphomechanics, *Philosophical Transactions of the Royal Society A: Mathematical, Physical and Engineering Sciences* **367,** 3555–3583 (2009).

51. Nardinocchi, P. & Teresi, L., On the active response of soft living tissues, *Journal of Elasticity* **88,** 27–39 (2007).

52. Fattal, R. & Kupferman, R., Constitutive laws for the matrix-logarithm of the conformation tensor, *Journal of Non-Newtonian Fluid Mechanics* **123,** 281–285 (2004).

53. Giusteri, G. G. & Seto, R., A theoretical framework for steady-state rheometry in generic flow conditions, *Journal of Rheology* **62,** 713–723 (2018).

54. Maklad, O. & Poole, R., A review of the second normal-stress difference; its importance in various flows, measurement techniques, results for various complex fluids and theoretical predictions, *Journal of Non-Newtonian Fluid Mechanics* **292,** 104522 (2021).

55. White, J. & Metzner, A., Development of constitutive equations for polymeric melts and solutions, *Journal of Applied Polymer Science* **7,** 1867–1889 (1963).

56. Haward, S. J. & McKinley, G. H., Stagnation point flow of wormlike micellar solutions in a microfluidic cross-slot device: Effects of surfactant concentration and ionic environment, *Physical Review E* **85,** 031502 (2012).

57. Varchanis, S., Haward, S. J., Hopkins, C. C., Tsamopoulos, J. & Shen, A. Q., Evaluation of constitutive models for shear-banding wormlike micellar solutions in simple and complex flows, *Journal of Non-Newtonian Fluid Mechanics* **307,** 104855 (2022).

58. Vasquez, P. A., McKinley, G. H. & Cook, L. P., A network scission model for wormlike micellar solutions: I. Model formulation and viscometric flow predictions, *Journal of non-newtonian fluid mechanics* **144,** 122–139 (2007).

59. Meissner, J., Basic parameters, melt rheology, processing and end-use properties of three similar low density polyethylene samples, *Pure and Applied Chemistry* **42,** 551–612 (1975).

60. Ferrás, L., Morgado, M., Rebelo, M., McKinley, G. H. & Afonso, A., A generalised Phan–Thien—Tanner model, *Journal of Non-Newtonian Fluid Mechanics* **269,** 88–99 (2019).

61. Dealy, J. M., Weissenberg and Deborah Numbers – Their Definition and Use, *Rheology Bulletin* **79,** 14–18 (2010).

62. Quarteroni, A. & Quarteroni, S., *Numerical models for differential problems* (Springer, 2014).